

Semiflexible Oligomers Crystallize via a Cooperative Phase Transition

Pierre Kawak,¹ Dakota S. Banks,¹ and Douglas R. Tree¹

Department of Chemical Engineering, Brigham Young University, Provo, Utah

(*Electronic mail: tree.doug@byu.edu.)

(Dated: 1 November 2021)

Semicrystalline polymers are ubiquitous, yet despite their fundamental and industrial importance, the theory of homogeneous nucleation from a melt remains a subject of debate. A key component of the controversy is that polymer crystallization is a non-equilibrium process, making it difficult to distinguish between effects that are purely kinetic and those that arise from the underlying thermodynamics. Due to computational cost constraints, simulations of polymer crystallization typically employ non-equilibrium molecular dynamics techniques with large degrees of undercooling that further exacerbate the coupling between thermodynamics and kinetics. In a departure from this approach, in this study we isolate the near-equilibrium nucleation behavior of a simple model of a melt of short, semiflexible oligomers. We employ several Monte Carlo methods and compute a phase diagram in the temperature–density plane along with two-dimensional free energy landscapes (FELs) that characterize the nucleation behavior. The phase diagram shows the existence of ordered nematic and crystalline phases in addition to the disordered melt phase. The minimum free energy path in the FEL for the melt–crystal transition shows a cooperative transition, where nematic order and monomer positional order move in tandem as the system crystallizes. This near-equilibrium phase transition mechanism broadly agrees with recent evidence that polymer stiffness plays an important role in crystallization, but differs in the specifics of the mechanism from several recent theories. We conclude that the computation of multidimensional FELs for models that are larger and more fine-grained will be important for evaluating and refining theories of homogeneous nucleation for polymer crystallization.

Keywords: Polymer Crystallization; Oligomer Crystallization; Energy Landscape Theory; Minimum Free Energy Path; Semiflexible Polymers

I. INTRODUCTION

Developing a theory for polymer crystallization in a melt is an important and long-unsolved problem in polymer science. It has been known for decades that polymers do not completely crystallize, leaving the material out of equilibrium.^{1–3} Consequently, the properties of the semicrystalline material are dependent on its processing history,⁴ making a theory of crystallization both an interesting fundamental problem and a fruitful endeavor for the practical engineering of polymer materials.

It is not possible to provide a comprehensive summary of all of the theoretical approaches to polymer crystallization here, but several excellent references are available.^{1–3,5,6} To situate our work in the context of this large literature, we wish to make two salient observations. First, a complete understanding of polymer crystallization must encompass both (i) the primary nucleation process that initiates crystallization and (ii) the subsequent crystal growth process.^{6–8} While it is widely understood that both of these kinetic processes require different (but possibly related) theories, the distinctions in the literature between models of (i) and (ii) are not always clear. For example, the widely discussed Lauritzen–Hoffman theory is a model of the crystal growth process that includes a “secondary nucleation” event that is distinct from the primary nucleation process.^{9,10} To limit our

scope and because of its foundational importance, we focus here on understanding (i) the primary nucleation process.

Second, despite more than a half-century of research on polymer crystallization, an attempt to ground the theory of polymer crystallization in concepts of modern polymer physics is a much more recent endeavor.^{11–17} For example, the classical theory of primary nucleation treats crystallization in a solution and a melt as mechanically equivalent,¹ and the role of polymer entanglement has only recently become a topic of serious study.¹⁸ Our approach is inspired by this agenda, which we describe more specifically in the paragraphs that follow.

A. Theories of Homogeneous Nucleation from a Melt

The prevailing theory of (homogeneous) primary nucleation of a crystal in a melt is based upon an extension of classical nucleation theory, which we will label “classical nucleation theory for polymers” (CNTP).^{1,14,17} The familiar idea, schematized in Figure 1a, is that a melt cooled below its melting temperature T_m experiences a driving force towards crystallization but is impeded by a free energy barrier due to surface tension. From a polymer physics perspective, one imagines that as a bundle of chains crystallize, a local density fluctuation of n monomers creates a cylindrical nucleus of radius r and

length l .¹⁹ Presumably, these chains are folded because the nucleation event happens locally before the rest of the chain can relax, leading to the well-known lamellar crystal structure.

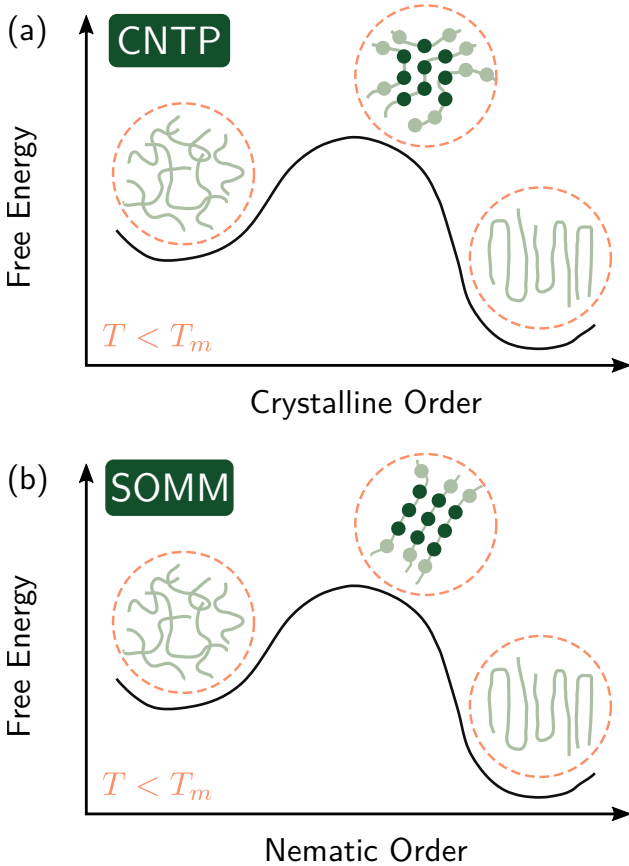


FIG. 1. (a) Classical nucleation theory for polymers (CNTP) postulates that the local positional ordering of monomers is the principal barrier to polymer crystallization. (b) By contrast, several new theories by Strobl, Olmsted, Milner, and Muthukumar (SOMM) propose that orientational alignment of the polymer chains is possibly a more important barrier.

There are a number of assumptions that undergird this relatively simple model of crystallization. First, the system is assumed to be near-equilibrium such that a suitable free-energy surface (i.e. a bulk free energy and surface tension) can be defined and related to bulk thermodynamic parameters. Additionally, one assumes that the kinetics are dictated by the free energy at the transition state, via typical arguments from transition state theory.¹⁷ Note that both of these two assumptions relegate the role of entanglement and other well-known aspects of polymer dynamics to secondary status in the theory.¹⁸ Additionally, CNTP assumes both a *specific shape* for the nucleus (typically a cylinder) and a *particular order parameter* (n , the number of monomers in the nucleus) for the kinetic pathway. All together, these assumptions constitute a very specific mechanism of crystallization: a

group of n monomers driven by *local* enthalpic and entropic interactions arrange into a crystalline lattice despite opposition from anisotropic cohesive interactions in the liquid.

Unfortunately, CNTP does not agree with at least two major qualitative experimental observations of melt crystallization. First, many polymers exhibit some type of intermediate state between the melt and crystalline states. n-alkane oligomers contain rotator phases between the melt and the crystalline phase,^{20–26} and several authors postulate their existence for polyethylene.^{13,26–30} Additionally, Keller and coworkers found an orthorhombic polyethylene crystal at elevated pressures and argued that it may exist as an intermediate state at normal conditions.^{31,32} Kaji and coworkers observed SAXS peaks before the appearance of WAXS Bragg peaks during the crystallization of poly(ethylene terephthalate), indicating the formation of ordered domains at longer length scales prior to crystallization.^{33,34} Similar observations have been made in scattering measurements on other polymers as well,^{35–38} although various interpretations have been given.³⁷ Second, many polymers exhibit “melt memory” (i.e. process history) effects which are not explainable by CNTP. Examples abound,^{39–41} but a prototypical case was observed in re-crystallization experiments on polypropylene by Li et al.^{42,43} When re-crystallizing, they observed process history effects on the semicrystalline morphology, nucleation rate, and crystal growth rate that depended on the degree of superheating ($T - T_m$) and holding time of the *prior melting step*.

With the above contradictory evidence, several researchers have proposed alternate theories to CNTP. Olmsted et al. theorized that a liquid-liquid phase gap lies *within* the liquid-crystal phase gap, and that a liquid-liquid spinodal decomposition coupled to the crystallization process could explain some of the anomalous scattering observations.¹⁶ Strobl proposed a multistep mechanism for crystallization, where the melt first transitions to an aligned mesophase before crystallizing.^{44–46} Along similar lines, Milner fleshed out a more specific quantitative theory of crystallization for polyethylene that includes an intermediate nematic rotator phase between the melt and the crystal.¹³ Muthukumar also used the idea of an intermediate state to construct a theory of polymer crystallization that includes melt-memory effects.⁴⁷

All of the above theories postulate a previously unrecognized role for chain connectivity, chain stiffness, and nematic ordering in the crystallization process. While each theory differs in its details, all postulate a key mechanistic difference: chain alignment must occur before monomers can order into a crystalline lattice. We refer to this idea as the SOMM (Strobl, Olmsted, Milner, Muthukumar) hypothesis for ease of reference. This concept is illustrated in Figure 1b, which shows a free energy surface as a function of some nematic order parameter, rather than a crystalline order parameter. Unlike the sur-

face energy explanation in CNTP, the free energy barrier in this case is primarily due to the entropy lost when chains align.

B. Simulation Studies of Homogeneous Nucleation

Simulations play an important complimentary role to theories of homogeneous nucleation, and in principle, detailed molecular simulations should be able to distinguish whether polymers crystallize with the mechanisms described by CNTP or by the theories of SOMM. Unfortunately, homogeneous nucleation is a rare event,⁴⁸ and brute force calculations can be exceptionally expensive when combined with the large densities and long polymer chains that typically accompany simulations of a polymer melt. Consequently, simulations of polymer crystallization typically employ non-equilibrium molecular dynamics (NEMD) techniques with large degrees of undercooling to accelerate nucleation.

As we describe below, the use of artificially accelerated kinetics have complicated the simulation evidence for and against various nucleation theories. In particular, large magnitudes of undercooling move the system further from equilibrium and amplify purely kinetic effects such as entanglement. While kinetic effects are widely believed to be important in polymer crystallization—though perhaps not to the degree seen in NEMD simulations—many differences between CNTP and SOMM rely on the presence of additional thermodynamic regimes, such as nematic phases, that complicate the interpretation of these simulations.

Thus, conventional NEMD methodologies have led to a situation where competing explanations are possible. For example, Yi, Rutledge, and co-workers did pioneering work using united-atom coarse-grained models of n-alkanes and polyethylene and found results broadly agreeing with CNTP, including observation of a cylindrical shape for the critical nucleus.^{17,49,50} Luo and Sommer describe a more nuanced story for melts of polyvinyl alcohol above the entanglement molecular weight. CNTP generally describes the nucleation behavior in their simulations, but entanglement gives rise to important thermal history/melt-memory effects.^{18,51,52}

By contrast, a number of other simulations have found qualitative support for the SOMM hypothesis. Wentzel and Milner performed all-atom simulations of n-alkanes and found two orientationally-ordered rotator phases in addition to an atomistically-ordered crystalline phase.²⁶ Using simulations of C50 and C1000 polyethylene and self-consistent field theory, Zhang and Larson⁵³ found a metastable nematic phase present for supercooled polyethylene that accelerated the crystallization kinetics with sufficient undercooling. Similarly, Hall et al. simulated a polyethylene melt and found crystals residing in nematic droplets, meaning the crystalline phase was pre-

ceded both temporally and spatially by nematic ordering.^{54–56} Additionally, Hall et al. found direct evidence that the shape of the nucleus was not a simple cylinder or sphere.⁵⁴ Recently, Nicholson and Rutledge also found direct evidence of the importance of nematic alignment for crystallization in a study of flow-enhanced nucleation of polyethylene.^{57,58}

Our approach departs from the NEMD approach that has led to the present controversy, and instead focuses on characterizing the phase behavior and *near-equilibrium* nucleation kinetics of a model polymer system. It may appear counter-intuitive to focus on near-equilibrium behavior, given that kinetic effects are widely believed to be important in polymer crystallization. However, a careful characterization of the underlying thermodynamics is an important fundamental step to resolving the questions raised by SOMM and, based on our review of the literature, has been neglected. More importantly, both CNTP and the theories by SOMM are *near-equilibrium theories*. In other words, they both rely on specific postulates of a free energy landscape (FEL) and order parameters that dictate the kinetic pathway. Accordingly, one way to qualitatively and quantitatively test these theories is to directly calculate the FEL for a model system.

Despite the numerous simulations cited above, relatively few studies have calculated values of the free energy of nucleation,^{17,59} and none have done so using both crystalline and nematic order parameters. Liu et al.⁶⁰ constructed a multidimensional polymer FEL using NEMD, but their primary focus was the relative stability of different solid phases and not the problem of polymer crystal nucleation. The most rigorous studies of the free energies of equilibrium crystal nucleation in a melt to date have been performed by Shakriov and Paul using a very simple model of semiflexible oligomers.^{61,62} Because calculating the full density of states for even this system proved too costly, Shakriov and Paul were forced to stop short of calculating a full phase diagram—resorting to a well-informed estimate—and they did not compute free energy surfaces or consider nucleation. However, they did provide meaningful insight into the role of attractive interactions, showing that attractions lead to only a small quantitative shift in the relevant phase boundaries.

In this work, we pick up where Shakriov and Paul left off in investigating the nucleation behavior of a melt of semiflexible oligomers as a methodological proof-of-principle and a pre-cursor to similar calculations for more realistic models of polymer crystallization. Accordingly, we use multiple Monte Carlo simulation techniques to compute (i) a phase diagram and (ii) relevant FELs for a model system of semiflexible oligomers using order parameters that characterize both crystalline and nematic order. As stated previously, calculating both a phase diagram and free energy surfaces allows us to directly examine several assumptions in CNTP and SOMM

for the system of oligomers, including explicit consideration of the nucleation mechanism.

With this in mind, the paper proceeds as follows. We first describe the polymer model, our Monte Carlo simulation methods, and explain the relevant order parameters. We then describe the phase behavior of the model in terms of crystalline and nematic order parameters. The key results of the paper are a calculation of the FEL of the phase transitions with respect to these crystalline and nematic order parameters. Interestingly, these calculations show a *cooperative phase transition* that agrees with the qualitative principles underlying the theories by SOMM, but differs in the details of the phase transition mechanism. We then speculate on the implications of this result for crystallization in polymer systems more broadly.

II. METHODS

We use four different simulation methods to study the crystalline transition: traditional Markov-chain Monte Carlo (MCMC), Wang-Landau Monte Carlo (WLMC), umbrella-sampling Monte Carlo (USMC) and expanded ensemble density of states (EXEDOS) simulations. Figure 2 shows the connections between these different methods and their relationship to the data and figures in the paper. The first box in Figure 2 details the recipe used to build phase diagrams. MCMC simulations construct melting curves and locate phase transition temperatures as a function of density. WLMC simulations—which directly sample the density of states and more efficiently sample rare events such as crystallization—provide an independent measure of the phase boundaries and compliment the MCMC results.^{63,64} In addition to their use for computing a phase diagram, MCMC, WLMC and USMC also generate appropriate configurations for analysis and as initial conditions for EXEDOS simulations. Likewise, the second box in Figure 2 details the recipe for free energy analysis employed in this study. EXEDOS simulations build multidimensional FELs at the transition temperature along order parameters of interest.^{65–69} EXEDOS simulations are similar in spirit to the WLMC method, but they take place in an expanded ensemble that includes the order parameter of interest. We use the “multidimensional lowest energy” algorithm (MULE) recently developed by Fu et al.⁷⁰ to compute the minimum free energy pathway (MFEP) between local minima on our 2D FELs. These methods are described in more detail in II B and in the Supplementary Material.

In an effort to capture polymer behavior while also minimizing computational requirements, we choose a system of short, semiflexible oligomers that experience only hard-core repulsion. Following Shakirov and Paul, we do not include an attractive potential in our model, despite their potential importance for polymers that crys-

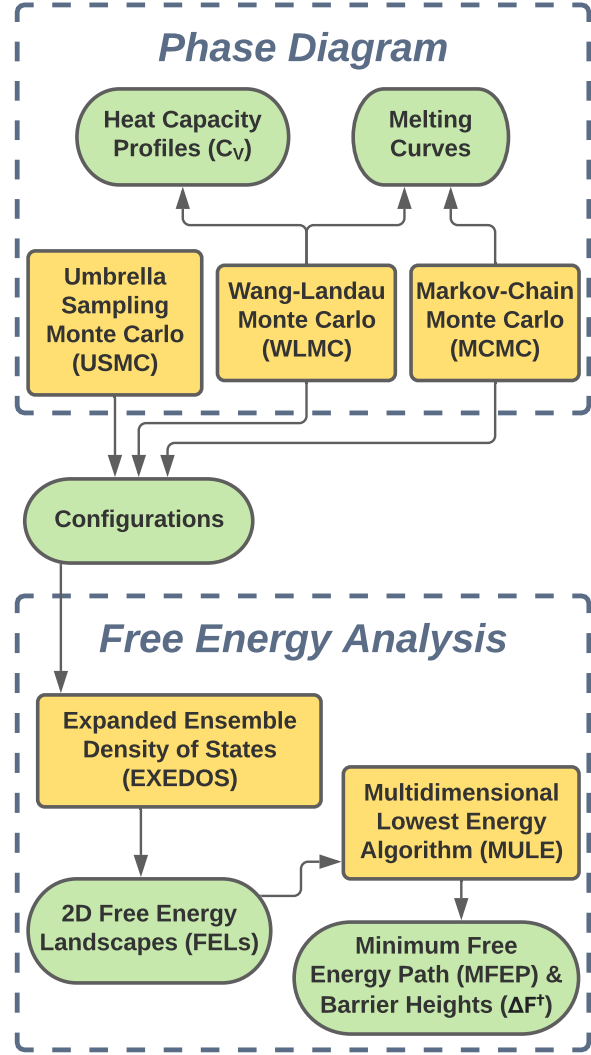


FIG. 2. Flowchart illustrating the connections between the methods used and the presented data. Yellow rectangles represent methods and green ovals correspond to one or more figures in the paper.

tallize.^{61,62} Shakriov and Paul found that attractive interactions induced only a minor shift in the phase boundary for the model in question,^{61,62} and their inclusion significantly increases the computational cost of our simulations. We believe that attractive interactions may indeed play a more important role for systems with softer potentials, but we leave such investigations to future work.

Consequently, in the present model, crystallization is driven by entropy not by energy.⁷¹ As shown below, the transition from an disordered melt to a nematically ordered crystal can happen either via densification at a constant temperature or via a temperature quench at a given density. In addition to reduced computational cost, this relatively simple system has additional advantages. It has a known ground state and crystal structure and the ex-

explicit inclusion of bending rigidity permits nematic alignment. The latter is important because it allows us to study both polymer connectivity and stiffness, both of which are important in more realistic models. More details of the polymer model are given in Section II A.

Note also that our choice of a hard-sphere model necessitates simulations in a constant volume (variable pressure) ensemble. Because most experiments are performed at constant pressure and variable density, the results presented here may be difficult to compare directly to such experiments.

Finally, in a system with both nematic and crystalline phases, there exists a 2D FEL with respect to changes in nematic and crystalline order. Accordingly, we employ two order parameters: P_2 for quantifying nematic alignment and the Steinhardt order parameter Q_6 for crystallinity. Additional information about these order parameters is given in II B and the Supplementary Material.

A. Polymer Model

The model consists of N_c chains containing N_b beads connected by bonds of a fixed length (σ) with a simple, step-wise bending stiffness potential

$$U_{\text{bend}}(\theta) = \begin{cases} -\varepsilon & \theta \leq \theta_s \\ 0 & \theta > \theta_s \end{cases} \quad (1)$$

where ε is the stiffness energy and θ_s is a cutoff angle. The stiffness potential is computed for all sets of three sequentially ordered beads forming a backbone angle of θ .

Non-bonded spheres interact through a hard-sphere potential

$$U_{\text{nb}}(r_{ij}) = \begin{cases} \infty & r_{ij} < \sigma \\ 0 & r_{ij} \geq \sigma \end{cases} \quad (2)$$

where $r_{ij} = |\mathbf{r}_j - \mathbf{r}_i|$ is the distance between two distally located beads. For all simulations in this paper, $N_c = 90$, $N_b = 10$, and $\cos(\theta_s) = 0.9$. These choices provide a system that is small enough to compute well-equilibrated FELs and enables a direct comparison to recent results by Shakirov and Paul.⁶¹ As discussed, the combination of the above two potentials gives the system a simply computable ground state ($T = 0$) energy

$$U_{\text{min}} = N_c(N_b - 2)\varepsilon \quad (3)$$

when all N_c chains are aligned in a close-packed configuration.

The polymer volume fraction is an important determinant of system behavior. It is given by the hard sphere

volume fraction of the total number of beads in a cubic simulation box of size L ,

$$\phi = \frac{N_c N_b \pi \sigma^3 / 6}{L^3} \quad (4)$$

Our simulations span volume fractions $\phi \in [0.379, 0.471]$. For comparison, the volume fractions of random and maximum close-packed configurations of hard spheres are 0.64 and $\pi/(3\sqrt{2}) \approx 0.7405$, respectively.⁷²

This relatively simple model contains a single length-scale parameter, the hard sphere diameter and bond length σ , and a single-energy scale parameter, the stiffness energy scale ε . Unless otherwise noted, all results below are non-dimensionalized in terms of these two parameters. Additionally, dimensional analysis reveals that there are only two dimensionless groups that govern the phase behavior of the system: the volume fraction ϕ and the reduced temperature $T_r = kT/\varepsilon$, where k is Boltzmann's constant and T is the absolute temperature.

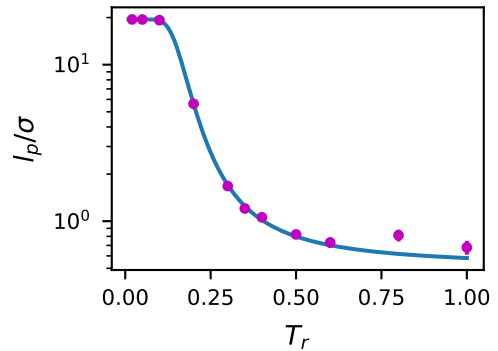


FIG. 3. Dimensionless persistence length, l_p/σ , versus reduced temperature, T_r , for a Monte Carlo simulation of a melt of phantom chains (magenta points) compared a theoretical estimate of a freely jointed chain (blue line). Error bars show the standard error of the mean.

Importantly, the combined group T_r implies that temperature and stiffness are coupled. To quantify this observation, Figure 3 shows the dimensionless persistence length l_p/σ as a function of T_r for an ideal version of the model, i.e. a version of the model with $U_{\text{nb}} = 0$. The persistence length, l_p , is obtained from the bond correlation function, $\langle \cos \theta(s) \rangle$, which is the average cosine of the angle between any two segments in the same chain separated by s bonds. The bond correlation function is assumed to decay exponentially as a function of distance s along the polymer backbone,

$$\langle \cos \theta(s) \rangle = \exp(-s\sigma/l_p) \quad (5)$$

and l_p/σ is obtained from a fit to this functional form. For comparison, the persistence length from simulation is compared to the theoretical prediction of a freely jo-

tating chain,

$$\frac{l_p}{\sigma} = \frac{1}{2} \left[\frac{1 + \langle \cos \theta(0) \rangle}{1 - \langle \cos \theta(0) \rangle} \right] \quad (6)$$

where $\langle \cos \theta \rangle$ is given by

$$\langle \cos \theta(0) \rangle = \frac{1}{2} \frac{\exp(1/T_r) \sin^2 \theta_s + \cos^2 \theta_s - \cos^2 \theta_m}{\exp(1/T_r)(1 - \cos \theta_s) + \cos \theta_s - \cos \theta_m} \quad (7)$$

and $\theta_m = 180^\circ$ is the maximum angle in phantom chain simulations⁶¹.

As shown in Figure 3, l_p/σ starts at or below the bond length $l_p/\sigma \approx 1$ at high T_r and monotonically increases to $l_p/\sigma \approx 20 = 2N_b$ as $T_r \rightarrow 0$. Consequently, chains at lower T_r are stiff and have a greater propensity to nematically align and to crystallize.

B. Simulations

To determine phase transition points for the phase diagram, we computed so-called melting curves using NVT-ensemble MCMC and constant-NV WLMC simulations. Melting curves consist of order parameters $P_2(T_r)$ and $Q_6(T_r)$ at fixed ϕ , and a phase transition (i.e. melting) takes place at a step-change in value of the order parameter. Melting curves get their name from an MCMC simulation that is initialized with either a nematic or crystalline configuration and then subjected to increasing temperatures until the system transitions to a disordered melt. One uses this procedure because MCMC simulations are inefficient at crossing barriers at first-order phase transitions, making it costly to compute the location of the transition. As an additional consequence of the difficulty of barrier-crossing, MCMC melting curves give an upper bound of the melting temperature. By contrast, WLMC has barrier-crossing properties that enable more efficient and more accurate calculations of first-order phase transitions. Our WLMC ‘‘melting curves’’ start from both ordered and disordered initial states and sample the entire temperature range simultaneously.

More specifically, MCMC melting curves were extracted from multiple simulations at equally-spaced values of temperature $T \in [0.1, 1]$. To ensure good statistics, each MCMC simulation was run for a length of approximately 1000 times the energy autocorrelation time ($\sim 10^6 - 10^7$ MC steps) and each data point on the curve was replicated eight times. WLMC melting curves were extracted from the density of states obtained using multi-windowed, multi-walker replica-exchange WLMC simulations. Each replica-exchange WLMC simulations utilized between 8 and 18 walkers and yielded density of states with $O(10^{-9})$ error. In both simulations, we employ a variety of polymer-specific moves^{73–80} to ensure efficient equilibration of the polymer chains including:

kink,^{81,82} end-kink,⁸² reptation,^{81,83} and configurational-bias versions of the same.^{73,74,76,80} Additional details regarding these methods are provided in the Supplementary Material.

To compute FELs, we used EXEDOS. EXEDOS is a modified WLMC approach that builds the FEL along a certain order parameter or reaction coordinate at a specific temperature and volume fraction.⁸⁴ EXEDOS has been previously used to construct an FEL along a variety of order parameters including distance,^{65,84,85} cut-off radii,⁸⁶ Steinhardt order parameters,⁶⁶ and nematic alignment.^{67,69} The free energy as a function of the order parameter θ (the FEL) is given by

$$F(\theta) = -kT \ln Z(\theta) + C \quad (8)$$

where C is an arbitrary constant and Z is the EXEDOS density of states. Recall that computing $F(\theta)$ permits a direct comparison to CNTP and SOMM predictions, as shown in Figure 1. In our calculations, we computed two-dimensional (2D) FELs from $Z(P_2, Q_6)$, using EXEDOS simulations that span two order parameters. High values of Q_6 indicate crystalline configurations whereas low values are characteristic of the disordered melt. Similarly, a value of P_2 closer to one indicates nematic alignment, whereas a value close to zero signifies a random distribution of chains. All EXEDOS simulations utilize replica-exchange with 8 to 18 walkers that are each initialized with different initial configurations and converge to a free energy with errors less than 10^{-7} in simulation units. In addition, each EXEDOS simulation was replicated three times and averaged to produce the final data. More details on EXEDOS simulations and the order parameters are provided in the Supplementary Material.

Our interest in the FEL extends to an analysis of its topological features with basins representing stable or metastable states and peaks representing rare events. Based on ideas from classical nucleation theory and transition state theory, we expect the MFEP between basins to be indicative of the kinetics of the system.⁸⁷ Similarly, we expect the maximum of the MFEP (a saddle point on the FEL surface) to characterize the primary barrier to nucleation. To find the MFEP and the saddle point, we used the MULE algorithm recently developed by Fu et al.⁷⁰ We use the resulting MFEP to calculate the barrier height between the saddle point and basins.

III. RESULTS

A. Equilibrium Phase Behavior

In order to understand the nucleation behavior of semiflexible oligomers, we must first understand their phase behavior. Accordingly, we used a combination of MCMC and WLMC simulations to study the melt–

nematic and melt–crystal phase transitions in order to construct a phase diagram.

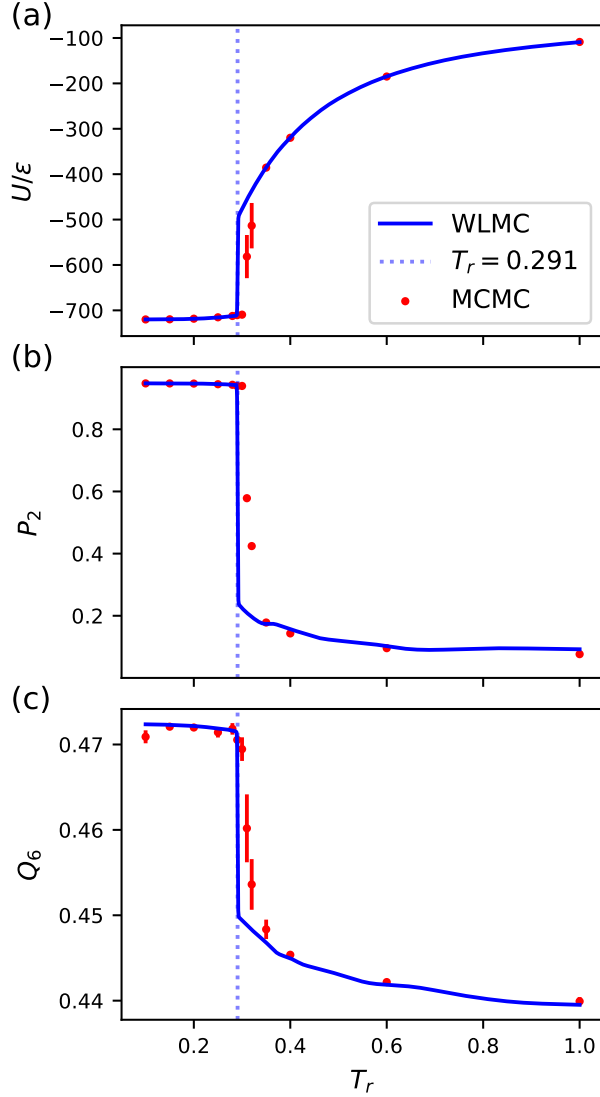


FIG. 4. Melting curves of the (a) internal energy, (b) nematic order parameter, (c) crystalline order parameter versus reduced temperature from MCMC (red points) and WLMC (blue line) at $\phi = 0.438$. The vertical dashed line is the best estimate of the melting temperature ($T_m = 0.291$). Error bars for MCMC data points depict the standard error of the mean.

Representative melting curves for the melt–crystalline transition at $\phi = 0.438$ for both methods are shown in Figure 4. The figure shows the potential energy U , the nematic order parameter P_2 , and the crystalline order parameter Q_6 versus T_r . All three melting curves show evidence of a first-order transition at the same temperature, as indicated by a sharp change in the order parameter at the melting temperature $T_r = T_m = 0.291$. As T_r increases, both P_2 and Q_6 decrease indicating that positional order and alignment both decrease upon melt-

ing. By contrast, U increases upon melting as the system gains conformational entropy at the expense of increased bending of chain backbones.

Importantly, the melting curves of U , P_2 and Q_6 in Figure 4 all change at the same temperature, revealing that there is only *one* transition as a function of T_r . As shown below, this is the case for all values of ϕ that we studied. Accordingly, in our simple system, there are no equilibrium intermediate states or multistep phenomena in the melt–crystal transition as theorized by Strobl,⁴⁵ though we must examine an FEL to rule out the possibility of metastable states.

It is also interesting to note that the WLMC simulations are generally more efficient and yield better statistics than the MCMC simulations. The latter are especially difficult to equilibrate at low temperatures and near the melting transition. Evidence of this loss in accuracy can be seen by the large error bars and the positive temperature shift in the MCMC data near T_m . This difficulty is apparent for all volume fractions but is exacerbated at higher values. Spontaneous crystallization from the melt is also difficult in MCMC simulations at higher ϕ making it harder to collect low T_r MCMC data. MCMC and WLMC melting curves at other values of ϕ appear in the Supplementary Material.

Focusing on the WLMC data, Figure 5 shows melting curves for P_2 and Q_6 , and the constant volume heat capacity C_V for five different values of the volume fraction $\phi \in \{0.379, 0.407, 0.428, 0.438, 0.471\}$. All systems are an isotropic melt state at high T characterized by low values of both Q_6 and P_2 . At a specific T_r (T_m), a change in P_2 and Q_6 and a corresponding peak in C_V provide evidence of a single first-order phase transition for all values of ϕ . However, there are differences between the transitions at high- ϕ and low- ϕ , an indication that there are two different types of phase transitions.

At the larger volume fractions ($\phi = 0.438$ and $\phi = 0.471$), the phase transition is clearly between a melt and a crystalline phase. At T_m , there is a large and sharp increase in Q_6 , manifesting a significant change in positional ordering. Additionally, P_2 approaches its maximum value, which it must for a crystalline system, and C_V shows a sharp and pronounced peak.

By contrast, at the smaller volume fractions ($\phi = 0.379$ and $\phi = 0.407$) the transition is between a melt and a nematic phase. The most direct evidence is the small change in positional ordering indicated by Q_6 in Figure 5b. Indeed, the nematic ordering parameter P_2 still shows a pronounced change at the T_m , though the change is more gradual and approaches a smaller value. Interestingly, even the heat capacity curves in Figure 5c show a difference between the two transitions, with the melt–nematic transition giving a broader, less pronounced peak.

The remaining volume fraction $\phi = \phi_c = 0.428$ is at or near the melt–nematic–crystal triple point. We located

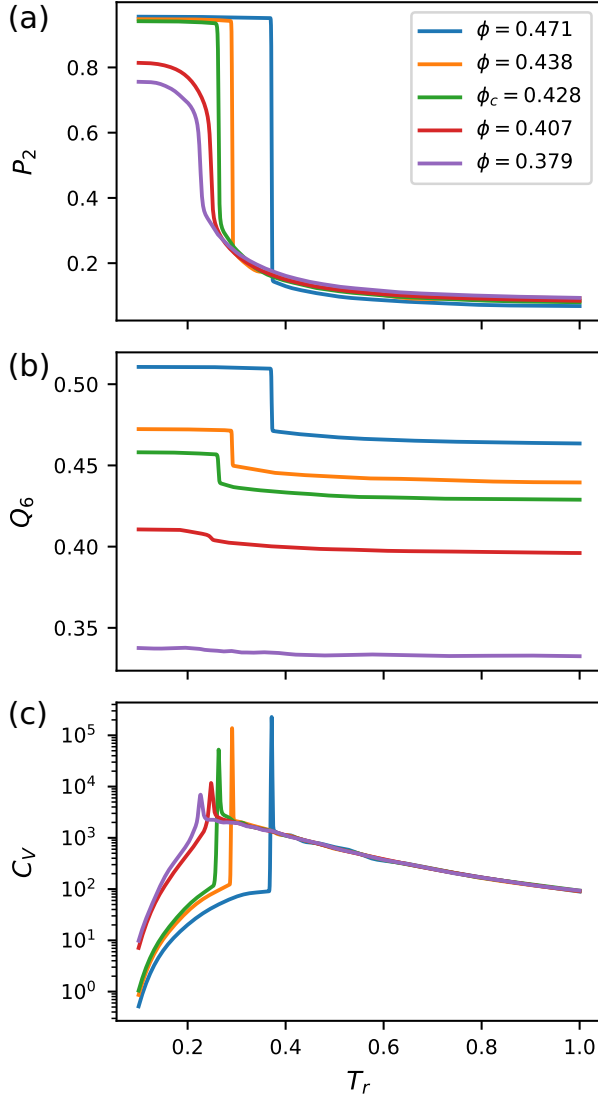


FIG. 5. WLMC simulation profiles of the (a) nematic order parameter, (b) crystallization order parameter and (c) heat capacity at $\phi \in \{0.379, 0.407, 0.428, 0.438, 0.471\}$.

ϕ_c by a trial-and-error process, creating melting curves at numerous values of ϕ with ϕ_c being the lowest volume fraction exhibiting a crystallization transition.

Additional information about the nature of the phases can be obtained by examining molecular configurations and structure factors, as shown in Figure 6. The melt phase, with a molecular configuration shown in Figure 6a-i, is made up of isotropically-oriented chains with no long-range positional ordering. The melt's structure factors, given in Figure 6a-ii, a-iii and a-iv, provide further evidence for these visual observations showing a circularly symmetric structure factor in all three dimensions characteristic of disordered systems. Additionally, there is a peak at the hard sphere radius ($q = 2\pi/\sigma$) characteristic of liquid structure.

TABLE I. Estimates of T_m from WLMC melting curves and EXEDOS simulations for five values of ϕ .

Transition Type	ϕ	T_m^{WLMC}	T_m^{EXEDOS}
Melt–Crystal	0.471	0.374	0.374
Melt–Crystal	0.438	0.291	0.291
Triple Point	0.428	0.263	0.267
Melt–Nematic	0.407	0.248	0.248
Melt–Nematic	0.379	0.226	0.226

As shown in a representative molecular configuration in Figure 6b-i, chains in the nematic phase are anisotropically oriented along a nematic director, but bead positions are not ordered in a crystal lattice. Again, structure factors provide supporting evidence for these visual observations. The structure factors in Figure 6b-ii and b-iii show anisotropy along q_x , characteristic of an aligned configuration with a director in the x -direction. The symmetric structure factor in the q_y – q_z plane is consistent with this interpretation. Additionally, the structure factors do not show evidence of long range positional order. There is a broad peak at $q_x = \pm 2\pi/\sigma$, along the nematic director, from positional ordering along the length of the chain. The peak in the q_y – q_z plane is at $\approx 2\pi/(1.1\sigma)$, indicating that the alignment in the x -direction has increased chain-chain spacing perpendicular to the director.

Finally, a characteristic molecular configuration of the crystalline phase is shown in Figure 6c-i, with chains showing both orientational and positional ordering. The structure factors in Figure 6c-ii, c-iii, and c-iv provide details about the nature of the crystal. Figure 6c-ii and c-iii indicate that, like the nematic phase, the chain axis of this crystal lies parallel to the x -axis and the peak at $q_x = 2\pi/\sigma$ indicates that (as expected) beads are regularly spaced at a distance of σ along the chain backbone. However, unlike the nematic phase, the chains are hexagonally ordered in the y – z plane, as indicated by the hexagonal scattering pattern looking down the nematic director in Figure 6c-iv. The hexagonal positional ordering in y and z is imperfect however, as indicated by peak smearing in Figures 6c-ii and c-iii. We believe this latter effect is due to an incommensurability between the crystal lattice and the (relatively small) box size. Further evidence that the simulation box is small comes from the appreciable cross pattern at low q due to Fraunhofer diffraction.⁸⁸

Using the melting and heat capacity curves above, we constructed a phase diagram in the ϕ – T_r plane in Figure 7. The melting temperatures for five densities of interest are also given in Table I. Isochores contain a single phase transition from a high-temperature disordered melt to either a low-temperature nematic phase or a low-temperature crystalline phase. Isotherms are more varied and include (i) a melt–nematic–crystal transition at low

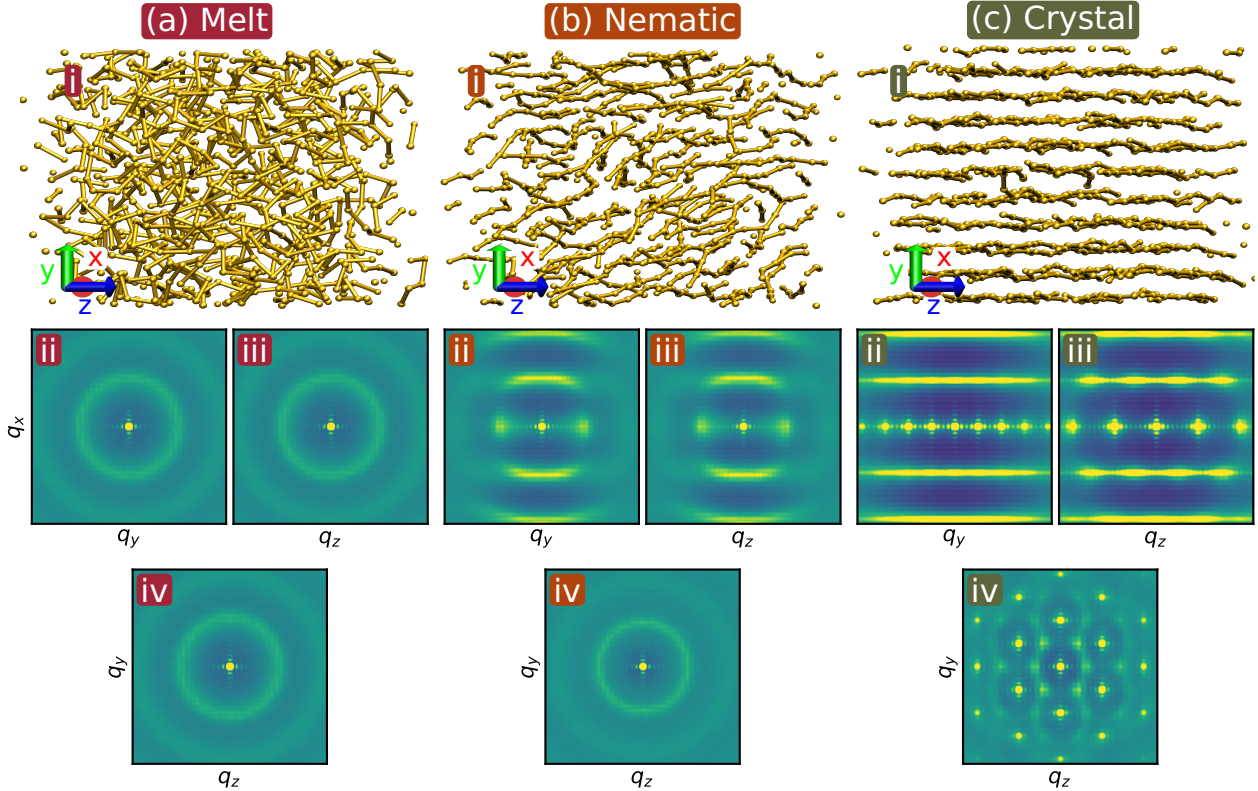


FIG. 6. (i) Representative MCMC snapshots of configurations and (ii-iv) averaged 2D structure factors for a (a) disordered melt phase at $\phi = 0.471$ and $T_r = 2.0$, (b) nematic phase at $\phi = 0.407$ and $T_r = 0.001$, and (c) crystal phase at $\phi = 0.471$ and $T_r = 0.001$. All q_i are in units of σ^{-1} and $q_x, q_y, q_z \in [-4.2\pi, 4.2\pi]$.

T_r and (ii) a melt–crystal transition at high T_r . Note that the existence of only a single phase transition along isochores implies that the the nematic–crystal transition line is isochoric. Indeed, WLMC simulations that bracket the triple-point volume fraction (data not shown) exhibit only a single phase transition, and additional EXEDOS simulations around the triple point (also not shown) narrow the range of the value of the triple point volume fraction to within $\pm O(10^{-2})$.

Shakirov and Paul predicted a phase diagram for the same model that differs in a few respects from Figure 7.⁶¹ Their theoretical prediction for the boundary between isotropic and aligned (nematic and crystalline) phases is shown in Figure 7 and is in fair agreement with our data. The slope of the prediction at low- ϕ appears similar, but the transition temperature is shifted to higher T_r relative to our observations of the melt–nematic transitions. More noticeably, their prediction fails to capture significant curvature that we observe at high- ϕ in the melt–crystal transition. In addition, our calculation of the triple point ($\phi = 0.428$) lies considerably outside the range of their estimate, $\phi \in [0.468, 0.478]$. One source of possible error in their predictions may be the reliance on a non-chain hard sphere equation-of-state that neglects the impact of connectivity.⁸⁹ As is always the case in sim-

ulations, our data may also suffer from sampling errors, though we have scrupulously tested for such errors.

B. Free Energy Landscape

Having constructed a phase diagram, we then examined the nucleation behavior of the system of semiflexible oligomers. We did so through the construction of FELs as a function of the order parameters P_2 and Q_6 in multidimensional EXEDOS simulations. Figure 8 shows FELs as a function of P_2 and Q_6 for the same five densities in Table I. FELs are temperature-dependent, and we show the FELs at their respective coexistence temperatures as given in Table I.

In an FEL, each local minimum (dark blue basins in Figure 8) represents a stable or metastable phase, with the global minimum giving the thermodynamically preferred phase. At the coexistence temperature, the two local minima (representing the two coexisting phases) should have equal values of the free energy. To find this value using EXEDOS, we swept temperature at constant ϕ around the value of T_m obtained from the melting curves above, until we found basins with equal free energies. As is apparent in Table I, T_m estimates from melting

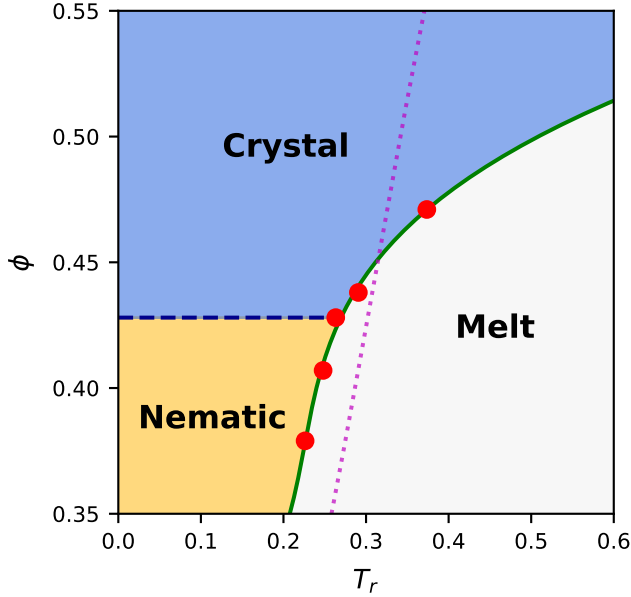


FIG. 7. Phase diagram for semiflexible oligomers in the ϕ – T_r plane. The high-temperature phase is a disordered melt (off white), the low-temperature, low-density phase is a nematic (yellow), and the low-temperature, high-density phase is a crystal (light blue). Red points are from melting curves and heat capacities, and the green line is a cubic best-fit curve estimate of the order-disorder transition (ODT). The dashed dark blue line of demarcation between the nematic and crystalline phases intersects the ODT at the triple point at $\phi = 0.428$ and $T_r = 0.263$. The dashed magenta line is a prediction of the ODT by Shakirov and Paul.⁶¹

curves and EXEDOS simulations agree very well, with a slight deviation ($\Delta T_r = 0.004$) at the triple point only. We speculate that the latter is due to a small error in our estimate of ϕ_c , the volume fraction of the triple point.

As expected from the phase behavior, there are three qualitatively different FELs in Figure 8, corresponding to the three different types of transitions. The FELs at the lowest densities ($\phi = 0.379$ and $\phi = 0.407$), shown in Figure 8d-e, are characteristic of a melt–nematic transition. Here the two local minima that represent the coexisting melt and nematic phases are at equal values of the crystalline order parameter Q_6 but at different values of the nematic order parameter P_2 . The transition from the low- P_2 melt to the high- P_2 nematic has a small barrier and involves essentially no change in Q_6 . Note also the consistency between the order parameters at the minima in the FELs and the range that the order parameters span in the melting curves at T_m in Figure 5.

The highest two densities ($\phi = 0.438$ and $\phi = 0.471$) shown in Figure 8a-b, correspond to the melt–crystal transition. The basins corresponding to the melt are at low Q_6 and low P_2 , and those representing the crystal phase are at high Q_6 and high P_2 . Again, the values of the order parameters of the minima match those in

Figure 5 at T_m . The scale of the barrier is considerably larger (note the scale bars for the FELs), and the transition between minima involves a change in both Q_6 and P_2 . The latter is important mechanically. The melt–crystal transition in this system is *smooth and cooperative*, with nematic alignment and positional ordering occurring simultaneously. There are, for example, no intermediate metastable minima that might lead the system to first align and then crystallize (or vice versa).

The FEL at the triple point ($\phi = 0.428$) given in Figure 8c shows the existence of three minima: melt at the lowest value of P_2 , nematic at a larger value of P_2 , and the crystal at a yet larger value of P_2 as well as a larger Q_6 . Interestingly, the melt–nematic barrier appears smaller than the nematic–crystal barrier, consistent with the scales of the melt–nematic and melt–crystal transitions at other values of ϕ .

Greater insight into the nucleation behavior can be obtained by extracting the MFEP from the FEL. Figure 9a shows the MFEP connecting the melt and crystalline basins for the FEL at $\phi = 0.438$ obtained using the MULE algorithm described in Section II B. In Figure 9b the MFEP is plotted along a coordinate, ξ , tracing the arc-length of the path in Q_6 – P_2 space. The MFEPs for the other FELs are qualitatively similar and can be found in the Supplementary Material.

The MFEP traces a smooth path that minimizes the free energy through the saddle point connecting the basins of the melt and crystal phases. The MFEP shows no other local minima, confirming our earlier observation that the phase transition involves cooperative nematic alignment and positional ordering. From a molecular level perspective, these results indicate that molecular ordering into a close-packed lattice occurs simultaneously with chain alignment.

In addition to providing insight into the phase transition mechanism, the MFEPs also provide quantitative estimates of the transition barriers. The barrier, ΔF^\ddagger , is the difference in free energy between the maximum of the MFEP (the transition state) and the minima (the two coexisting phases). Figure 10 shows both the forward and reverse values of ΔF^\ddagger as a function of ϕ . These barrier heights were obtained from MFEPs derived from the FELs in Figure 8 similar to Figure 9 and are provided in the Supplementary Material. The forward (freezing) and reverse (melting) value of ΔF^\ddagger should be equal at the phase coexistence temperature, but the free energies are quite sensitive to even slight deviations from the melting temperature, sometimes leading to small differences (i.e. at $\phi = 0.471$). In addition to minor deviations from the coexistence temperature, the discrete size of the bins in the EXEDOS algorithm (i.e. in this case in the Q_6 dimension) can introduce errors into the FELs that propagate into the MFEPs the values of ΔF^\ddagger .

The nucleation barrier drastically increases as ϕ increases. For the lowest two values of ϕ (i.e. the systems

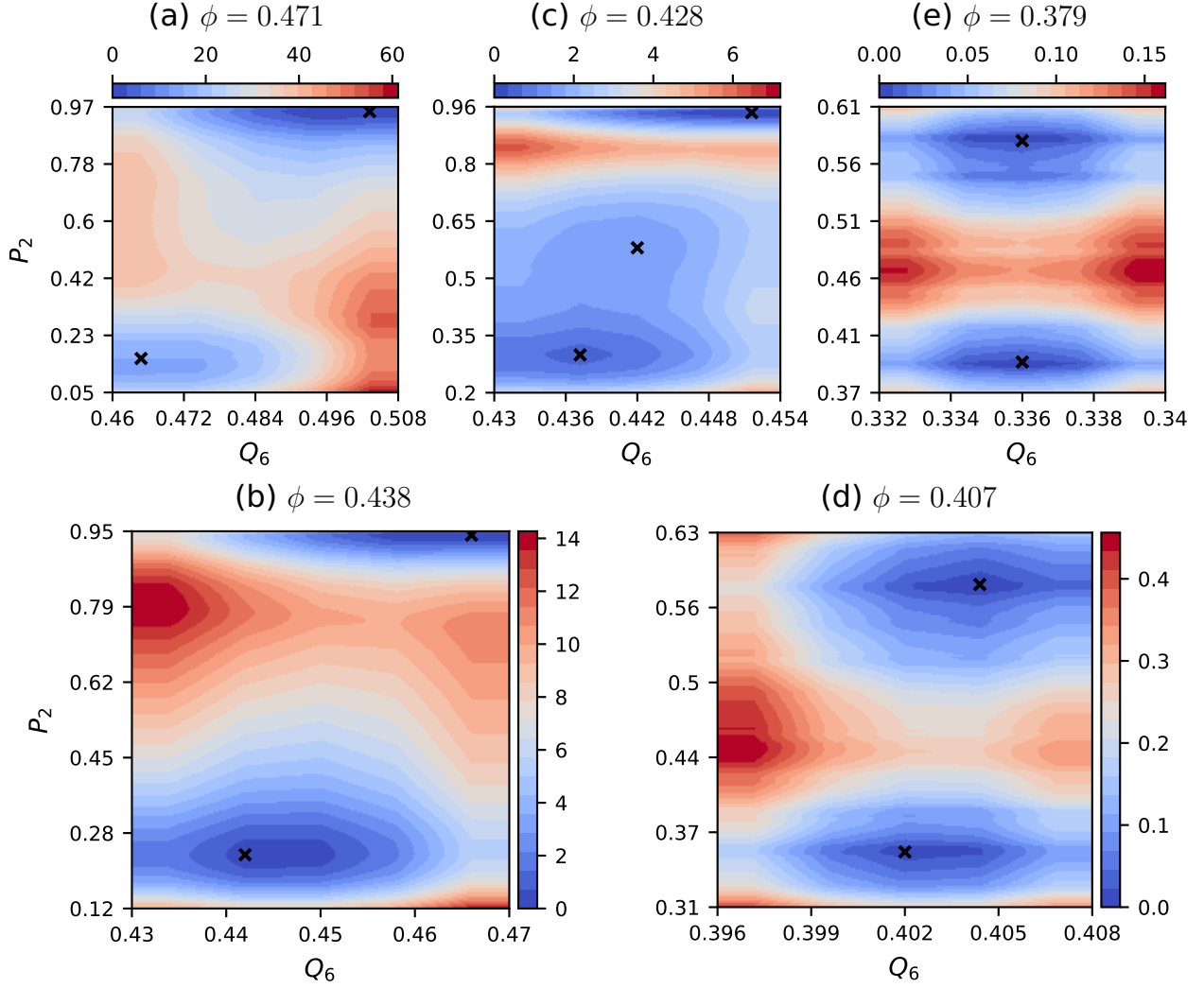


FIG. 8. FELs as a function of P_2 and Q_6 at $\phi \in \{0.471, 0.438, 0.428, 0.407, 0.379\}$ in (a)-(e), respectively. Free energy colormaps are in units of ϵ . Black x's denote locations of local minima. All FELs are obtained at their coexistence temperature as given in Table I.

with melt–nematic transitions) the barrier is small, and we can expect fast nucleation even at the melting temperature, T_m . At the largest values of ϕ (i.e. the systems with melt–crystal transitions) the barrier is large, and spontaneous nucleation at T_m is unlikely. This result qualitatively agrees with experimental observations that large induction times are required for polymer crystal nucleation experiments, even at large degrees of supercooling.^{33,34,37,38}

Interestingly, the triple point occurs when the barrier height is $O(\epsilon)$, where ϵ is the characteristic scale of the bending energy. We speculate that the triple point occurs when the density is large enough that the free energy cost to bending is similar to that for positional re-ordering. Thus, nematic ordering occurs at low ϕ when bending is cheap relative to positional ordering, and crystallization happens at high ϕ when bending is relatively costly.

IV. DISCUSSION AND CONCLUSION

We have studied the thermodynamic and crystal nucleation behavior of a model of semiflexible oligomers. Using a combination of MCMC and WLMC simulations, we have constructed a phase diagram in the ϕ – T_r plane that shows three phases: a melt, a nematic, and a crystalline phase. The melt–nematic phase transition is well-characterized by a classical nematic order parameter P_2 . By contrast, the melt–crystal phase transition is better characterized in a two-order parameter phase space of P_2 and Q_6 , the latter parameter characterizing positional order of monomers in a crystalline lattice. Accordingly, we built 2D P_2 – Q_6 FELs for various volume fractions, ϕ , at their transition temperatures to better understand nucleation pathways. To our knowledge, this is the first

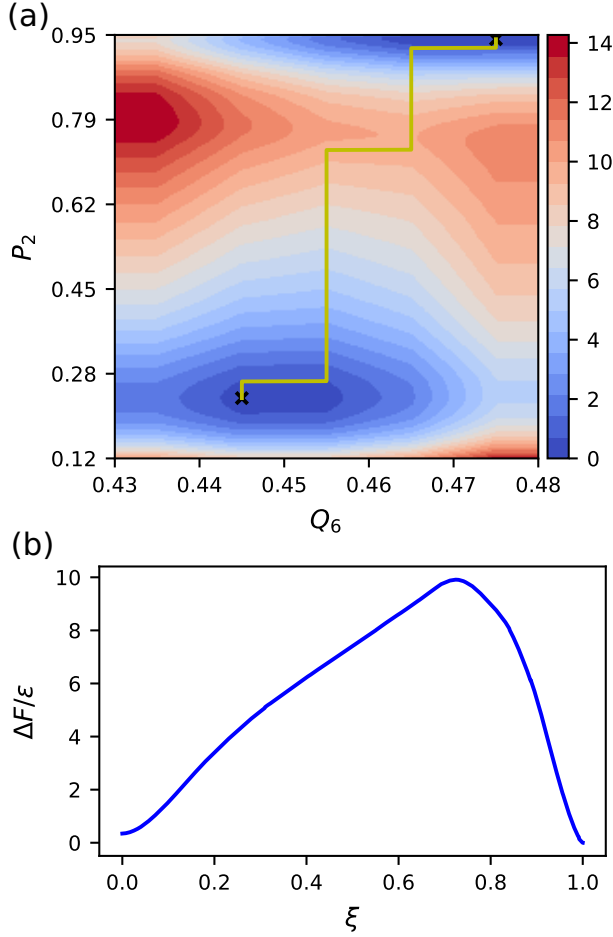


FIG. 9. (a) 2D Q_6 - P_2 FEL at $\phi = 0.438$ (identical to Figure 8b) with MULE-extracted MFEP in yellow. Discrete jumps in the MFEP are related to the discrete size of the bins along Q_6 . (b) MFEP values from the 2D Q_6 - P_2 FEL at $\phi = 0.438$ projected along the reaction coordinate of its arc-length in Q_6 - P_2 space.

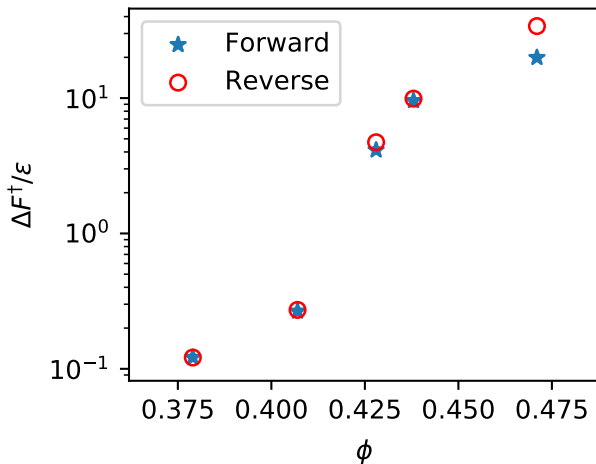


FIG. 10. Forward and reverse barrier heights, $\Delta F^\ddagger/\epsilon$, extracted from MFEPs as a function of ϕ .

2D FEL produced for a model of crystallizing polymers at equilibrium. The FELs reaffirmed the importance of both P_2 and Q_6 in the melt-crystal transition, and importantly, they showed that the MFEP of a melt-crystal transition involves a smooth and cooperative change in nematic alignment and positional ordering.

Our results are broadly consistent with principles underlying the SOMM hypothesis of polymer crystallization, but the details of the mechanism are unique. Recall that CNTP postulates that nucleation proceeds along a single, crystalline order parameter, as outlined in Figure 1. The SOMM hypothesis suggests that nematic order drives the transition, with some authors invoking an explicit intermediate stable or metastable phase. The MFEP in Figure 9 is a function of both order parameters, but depends much more strongly on the nematic order parameter. However, unlike specific theories by SOMM, the MFEP we calculate indicates a cooperative transition, rather than one that relies on intermediate phases or two-step process during nucleation.

Recent research on crystal nucleation outside of the field of polymers lends further support to our approach. Classical nucleation theory for simple molecules like Argon postulates a one-step process involving a single order parameter. Unfortunately, this simple model predicts nucleation rates that disagree with experimental values by 26 orders of magnitude!⁹⁰ The assumption of a simple reaction coordinate also fails to describe the transition path, and there is ample evidence for alternative nucleation pathways.⁹¹⁻⁹⁵ More complex molecules like water are also (unsurprisingly) poorly predicted by classical nucleation theory.⁹⁶⁻⁹⁸ Additional studies on the crystallization of multi-atomic molecules further suggests that transition pathways consisting of multiple order parameters are likely the norm rather than the exception.⁹⁹⁻¹⁰²

Based on our observation of cooperativity between nematic and positional order, we speculate that the temperature dependence of chain stiffness plays an important and underappreciated role in polymer crystallization. Indeed, this claim is bolstered by a recent simulation by Zhang and Larson showing that supercooled polyethylene possesses a metastable nematic phase.⁵³ Accordingly, we believe that chain semiflexibility is an important factor for a polymer-physics based theory of primary nucleation.

Despite the suggestive nature of our results, more work remains to be done to see if the cooperative mechanism is a general phenomenon. The present model is small, consists of short chains with only a few Kuhn lengths, and has an overly-simplistic potential compared to atomic systems. Calculations with a larger system will provide insight into the question of the nucleus shape, and longer chains will be necessary to observe folded lamellar crystals. A more realistic interatomic potential will allow quantitative predictions that can be compared with experimental systems.

Nevertheless, there are reasons to believe that the present conclusions are more broadly applicable than may first appear. Using a similar system, Shakirov and Paul recently claimed that molecular weight produces relatively small changes to the phase diagram.⁶¹ They also provided evidence that attractive interactions produce no additional phases, only introducing a shift to the transition temperatures.^{61,62} There is also simulation evidence in the literature on polyethylene and rotator phases that suggests that molecular weight is relatively unimportant to the process of nucleation beyond a certain threshold.^{17,49,50,103–107} Specifically, it was observed that the size of the critical nucleus is independent of chain lengths surpassing two Kuhn lengths of the model polymer.

Going forward, it will be fruitful to compare both molecular dynamics simulations and experiments to kinetic predictions based on MFEPs and barrier heights from this and related models. Barriers based on MFEPs are entirely due to thermodynamics, and induction times

$$\tau \sim \exp(-\Delta F^\ddagger/kT) \quad (9)$$

can be estimated using transition state theory. By contrast, both experiments and molecular dynamics may contain additional kinetic effects due to diffusion and chain entanglement. Therefore, comparisons may enable one to distinguish between near-equilibrium and dissipative phenomena.

Ultimately, we anticipate increased insight will come from extending these methods to larger systems with longer chains and more complex potentials. Based on their work with WLMC, Shakirov and Paul⁶¹ have suggested that reaching large system sizes and attraction energies might be exceedingly costly. However, EXEDOS does not experience the same cost scaling problems as WLMC, and can be used to generate similar information. Therefore, future comparisons between the results of EXEDOS simulations as well as experimental work and molecular dynamics simulations should allow for a more comprehensive look into theories of polymer crystallization.

LIST OF SYMBOLS AND ACRONYMS

- **FEL**: free energy landscape
- **CNTP**: classical nucleation theory for polymers
- T_m : melting/coexistence temperature
- **SAXS**: small angle X-ray scattering
- **WAXS**: wide angle X-ray scattering
- **SOMM**: Strobl-Olmsted-Milner-Muthukumar theories

- **NEMD**: non-equilibrium molecular dynamics
- **MCMC**: Markov-chain Monte Carlo
- **WLMC**: Wang-Landau Monte Carlo
- **EXEDOS**: expanded ensemble density of states
- **MFEP**: minimum free energy pathway
- **MULE**: multidimensional lowest energy algorithm
- P_2 : nematic order parameter
- Q_6 : crystalline Steinhardt order parameter
- N_c : number of chains
- N_b : chain length (number of hard sphere beads in chain)
- σ : hard sphere bead diameter and bond length and simulation length scale unit
- ϵ : stiffness energy scale and simulation energy scale unit
- ϕ : hard sphere volume fraction
- L : cubic simulation box size
- T_r : reduced temperature = kT/ϵ
- l_p : persistence length
- U : potential energy
- C_V : constant volume heat capacity
- ΔF^\ddagger : free energy barrier

SUPPLEMENTARY MATERIAL

The Supplementary Material contains a more detailed description of the methods and for additional figures on the MCMC, WLMC and EXEDOS results for all volume fractions studied.

ACKNOWLEDGMENTS

We gratefully acknowledge input and programming efforts by Andrew S. Gibson and Beverly Delgado to the early stages of this work as well as fruitful discussions with Qinyu Zhu and Rami Alhasan. Acknowledgment is also made to the donors of The American Chemical Society Petroleum Research Fund (PRF# 59244-DNI6) for support of this research. Finally, we acknowledge computational resources from the Office of Research Computing at Brigham Young University.

DATA AVAILABILITY STATEMENT

The data that support the findings of this study are available from the corresponding author upon reasonable request.

- ¹J. M. Schultz, *Polymer Crystallization: The development of crystalline order in thermoplastic polymers* (Oxford University Press and the American Chemical Society, 2001).
- ²L. Mandelkern, *Crystallization of Polymers: Volume 1 Equilibrium Concepts*, 2nd ed. (Cambridge University Press, 2002).
- ³L. Mandelkern, *Crystallization of Polymers: Volume 2 Kinetics and Mechanisms*, 2nd ed. (Cambridge University Press, 2004).
- ⁴Y. Nie, H. Gao, M. Yu, Z. Hu, G. Reiter, and W. Hu, "Competition of crystal nucleation to fabricate the oriented semi-crystalline polymers," *Polymer* **54**, 3402–3407 (2013).
- ⁵K. Armitstead, G. Goldbeck-Wood, and A. Keller, "Polymer crystallization theories," in *Macromolecules: Synthesis, Order and Advanced Properties* (Springer-Verlag, 1992) pp. 219–312.
- ⁶M. Zhang, B.-H. Guo, and J. Xu, "A Review on Polymer Crystallization Theories," *Crystals* **7**, 4 (2016).
- ⁷X. Tang, W. Chen, and L. Li, "The Tough Journey of Polymer Crystallization: Battling with Chain Flexibility and Connectivity," *Macromolecules* **52**, 3575–3591 (2019).
- ⁸B. Lotz, T. Miyoshi, and S. Z. D. Cheng, "50th Anniversary Perspective: Polymer Crystals and Crystallization: Personal Journeys in a Challenging Research Field," *Macromolecules* **50**, 5995–6025 (2017).
- ⁹J. I. Lauritzen and J. D. Hoffman, "Formation of polymer crystals with folded chains from dilute solution," *J. Chem. Phys.* **31**, 1680–1681 (1959).
- ¹⁰A. Bourque, C. R. Locker, and G. C. Rutledge, "Molecular Dynamics Simulation of Surface Nucleation during Growth of an Alkane Crystal," *Macromolecules* **49**, 3619–3629 (2016).
- ¹¹M. Muthukumar, "Trends in polymer physics and theory," *Prog. Polym. Sci.* **100**, 101184 (2020).
- ¹²P. Welch and M. Muthukumar, "Molecular Mechanisms of Polymer Crystallization from Solution," *Phys. Rev. Lett.* **87**, 218302 (2001).
- ¹³S. T. Milner, "Polymer crystal-melt interfaces and nucleation in polyethylene," *Soft Matter* **7**, 2909–2917 (2011).
- ¹⁴J. U. Sommer, "Theoretical aspects of the equilibrium state of chain crystals," in *Lecture Notes in Physics*, Lecture Notes in Physics, Vol. 714 (Springer, 2007) Chap. 2, pp. 19–45.
- ¹⁵G. Strobl, "The Semicrystalline State," in *The Physics of Polymers* (Springer Berlin Heidelberg, Berlin, Heidelberg, 2007) Chap. 5, pp. 165–222.
- ¹⁶P. D. Olmsted, W. C. Poon, T. C. McLeish, N. J. Terrill, and A. J. Ryan, "Spinodal-assisted crystallization in polymer melts," *Phys. Rev. Lett.* **81**, 373–376 (1998).
- ¹⁷P. Yi and G. C. Rutledge, "Molecular simulation of crystal nucleation in n-octane melts," *J. Chem. Phys.* **131**, 134902 (2009).
- ¹⁸C. Luo and J.-U. Sommer, "Disentanglement of Linear Polymer Chains Toward Unentangled Crystals," *ACS Macro Lett.* **2**, 31–34 (2013).
- ¹⁹Some researchers define a spherical nucleus and reach qualitatively similar conclusions. For the sake of brevity, we will only discuss the more common cylindrical case.
- ²⁰G. Ungar, "Structure of rotator phases in n-alkanes," *J. Phys. Chem.* **87**, 689–695 (1983).
- ²¹E. B. Sirota, H. E. King, D. M. Singer, and H. H. Shao, "Rotator phases of the normal alkanes: An x-ray scattering study," *J. Chem. Phys.* **98**, 5809–5824 (1993).
- ²²E. B. Sirota and D. M. Singer, "Phase transitions among the rotator phases of the normal alkanes," *J. Chem. Phys.* **101**, 10873–10882 (1994).
- ²³E. B. Sirota, "Remarks concerning the relation between rotator phases of bulk n-alkanes and those of Langmuir monolayers of alkyl-chain surfactants on water," *Langmuir* **13**, 3849–3859 (2002).
- ²⁴E. B. Sirota and A. B. Herhold, "Transient phase-induced nucleation," *Science* **283**, 529–532 (1999).
- ²⁵A. Marbeuf and R. Brown, "Molecular dynamics in n-alkanes: Pre-melting phenomena and rotator phases," *J. Chem. Phys.* **124**, 54901 (2006).
- ²⁶N. Wentzel and S. T. Milner, "Crystal and rotator phases of n-alkanes: A molecular dynamics study," *J. Chem. Phys.* **132**, 0–10 (2010).
- ²⁷E. Sirota and A. Herhold, "Transient rotator phase induced nucleation in n-alkane melts," *Polymer* **41**, 8781–8789 (2000).
- ²⁸H. Kraack, M. Deutsch, and E. B. Sirota, "N-alkane homogeneous nucleation: Crossover to polymer behavior," *Macromolecules* **33**, 6174–6184 (2000).
- ²⁹H. Kraack, E. B. Sirota, and M. Deutsch, "Homogeneous crystal nucleation in short polyethylenes," *Polymer* **42**, 8225–8233 (2001).
- ³⁰E. B. Sirota, "Polymer crystallization: Metastable mesophases and morphology," *Macromolecules* **40**, 1043–1048 (2007).
- ³¹S. Rastogi, M. Hikosaka, H. Kawabata, and A. Keller, "Role of mobile phases in the crystallization of polyethylene. I. Metastability and lateral growth," *Macromolecules* **24**, 6384–6391 (1991).
- ³²A. Keller, M. Hikosaka, S. Rastogi, A. Toda, P. J. Barham, and G. Goldbeck-Wood, "An approach to the formation and growth of new phases with application to polymer crystallization: effect of finite size, metastability, and Ostwald's rule of stages," *J. Mater. Sci.* **29**, 2579–2604 (1994).
- ³³M. Imai, K. Kaji, T. Kanaya, and Y. Sakai, "Chain conformation in the induction period of crystallization of poly(ethylene terephthalate)," *Phys. B (Amsterdam, Neth.)* **213-214**, 718–720 (1995).
- ³⁴M. Imai, K. Kaji, T. Kanaya, and Y. Sakai, "Ordering process in the induction period of crystallization of poly(ethylene terephthalate)," *Phys. Rev. B* **52**, 12696–12704 (1995).
- ³⁵N. Stribeck, U. Nöchel, A. Almedárez Camarillo, S. V. Roth, M. Dommach, and P. Bösecke, "SAXS study of oriented crystallization of polypropylene from a quiescent melt," *Macromolecules* **40**, 4535–4545 (2007).
- ³⁶G. Matsuba, K. Kaji, K. Nishida, T. Kanaya, and M. Imai, "Conformational change and orientation fluctuations prior to the crystallization of syndiotactic polystyrene," *Macromolecules* **32**, 8932–8937 (1999).
- ³⁷Z. G. Wang, B. S. Hsiao, E. B. Sirota, and S. Srinivas, "A simultaneous small- and wide-angle X-ray scattering study of the early stages of melt crystallization in polyethylene," *Polymer* **41**, 8825–8832 (2000).
- ³⁸K. Mita, H. Okumura, K. Kimura, T. Isaki, M. Takenaka, and T. Kanaya, "Simultaneous small- and wide-angle X-ray scattering studies on the crystallization dynamics of poly(4-methylpentene-1) from melt," *Polym. J.* **45**, 79–86 (2013).
- ³⁹A. Häfele, B. Heck, T. Hippler, T. Kawai, P. Kohn, and G. Strobl, "Crystallization of poly(ethylene-co-octene): II Melt memory effects on first order kinetics," *Eur. Phys. J. E* **16**, 217–224 (2005).
- ⁴⁰G. Hauser, J. Schmidtke, and G. Strobl, "The role of co-units in polymer crystallization and melting: New insights from studies on syndiotactic poly(propene-co-octene)," *Macromolecules* **31**, 6250–6258 (1998).
- ⁴¹J. Lu, H. Yang, Y.-x. Ji, X.-y. Li, Y. Lv, F.-m. Su, and L.-b. Li, "Strong Memory Effect of Metastable β Form *Trans*-1,4-Polyisoprene above Equilibrium Melting Temperature," *Macromol. Chem. Phys.* **218**, 1700235 (2017).
- ⁴²X.-y. Li, F.-m. Su, Y. Ji, N. Tian, J. Lu, Z. Wang, Z. Qi, and L.-b. Li, "Influence of the memory effect of a mesomorphic isotactic polypropylene melt on crystallization behavior," *Soft Matter* **9**, 8579 (2013).
- ⁴³X.-y. Li, Z. Ma, F.-m. Su, N. Tian, Y.-x. Ji, J. Lu, Z. Wang, and L.-b. Li, "New understanding on the memory effect of crystallized iPP," *Chin. J. Polym. Sci.* **32**, 1224–1233 (2014).

- ⁴⁴G. Strobl, "From the melt via mesomorphic and granular crystalline layers to lamellar crystallites: A major route followed in polymer crystallization," *Eur. Phys. J. E* **3**, 165–183 (2000).
- ⁴⁵G. Strobl, "A thermodynamic multiphase scheme treating polymer crystallization and melting," *Eur. Phys. J. E* **18**, 295–309 (2005).
- ⁴⁶G. Strobl, "Colloquium: Laws controlling crystallization and melting in bulk polymers," *Rev. Mod. Phys.* **81**, 1287–1300 (2009).
- ⁴⁷M. Muthukumar, "Communication: Theory of melt-memory in polymer crystallization," *J. Chem. Phys.* **145**, 31105 (2016).
- ⁴⁸C. Dellago and P. G. Bolhuis, "Transition Path Sampling and Other Advanced Simulation Techniques for Rare Events," in *Advanced Computer Simulation Approaches for Soft Matter Sciences III*, Vol. 221, edited by C. Holm and K. Kremer (Springer Berlin Heidelberg, 2009) pp. 167–233.
- ⁴⁹P. Yi and G. C. Rutledge, "Molecular simulation of bundle-like crystal nucleation from n-icosane melts," *J. Chem. Phys.* **135**, 24903 (2011).
- ⁵⁰P. Yi, C. R. Locker, and G. C. Rutledge, "Molecular dynamics simulation of homogeneous crystal nucleation in polyethylene," *Macromolecules* **46**, 4723–4733 (2013).
- ⁵¹C. Luo and J. U. Sommer, "Frozen topology: Entanglements control nucleation and crystallization in polymers," *Phys. Rev. Lett.* **112**, 195702 (2014).
- ⁵²C. Luo and J. U. Sommer, "Role of Thermal History and Entanglement Related Thickness Selection in Polymer Crystallization," *ACS Macro Lett.* **5**, 30–34 (2016).
- ⁵³W. Zhang and R. G. Larson, "A metastable nematic precursor accelerates polyethylene oligomer crystallization as determined by atomistic simulations and self-consistent field theory," *J. Chem. Phys.* **150**, 244903 (2019).
- ⁵⁴K. W. Hall, T. W. Sirk, S. Percec, M. L. Klein, and W. Shinoda, "Divining the shape of nascent polymer crystal nuclei," *J. Chem. Phys.* **151**, 144901 (2019).
- ⁵⁵K. W. Hall, T. W. Sirk, S. Percec, M. L. Klein, and W. Shinoda, "Monodisperse polymer melts crystallize via structurally polydisperse nanoscale clusters: Insights from polyethylene," *Polymers* **12**, 447 (2020).
- ⁵⁶K. W. Hall, S. Percec, W. Shinoda, and M. L. Klein, "Property Decoupling across the Embryonic Nucleus–Melt Interface during Polymer Crystal Nucleation," *J. Phys. Chem. B* **124**, 4793–4804 (2020).
- ⁵⁷D. A. Nicholson and G. C. Rutledge, "An assessment of models for flow-enhanced nucleation in an n-alkane melt by molecular simulation," *J. Rheol.* **63**, 465–475 (2019).
- ⁵⁸D. A. Nicholson and G. C. Rutledge, "Flow-induced inhomogeneity and enhanced nucleation in a long alkane melt," *Polymer* **200**, 122605 (2020).
- ⁵⁹Q. Chen, D. Kozuch, and S. T. Milner, "'Plunger' Method for Simulating Crystal-Melt Interfacial Free Energies," *Macromolecules* **50**, 4797–4806 (2017).
- ⁶⁰C. Liu, J. G. Brandenburg, O. Vålsson, K. Kremer, and T. Bereau, "Free-energy landscape of polymer-crystal polymorphism," *Soft Matter* **16**, 9683–9692 (2020).
- ⁶¹T. Shakirov and W. Paul, "Crystallization in melts of short, semi-flexible hard polymer chains: An interplay of entropies and dimensions," *Phys. Rev. E* **97**, 042501 (2018).
- ⁶²T. Shakirov, "Crystallisation in Melts of Short, Semi-Flexible Hard-Sphere Polymer Chains: The Role of the Non-Bonded Interaction Range," *Entropy* **21**, 856 (2019).
- ⁶³F. Wang and D. P. Landau, "Efficient, multiple-range random walk algorithm to calculate the density of states," *Phys. Rev. Lett.* **86**, 2050 (2001).
- ⁶⁴M. P. Taylor, W. Paul, and K. Binder, "Phase transitions of a single polymer chain: A Wang-Landau simulation study," *J. Chem. Phys.* **131**, 114907 (2009).
- ⁶⁵N. Rathore, Q. Yan, and J. J. de Pablo, "Molecular simulation of the reversible mechanical unfolding of proteins," *J. Chem. Phys.* **120**, 5781–5788 (2004).
- ⁶⁶M. Chopra, M. Müller, and J. J. de Pablo, "Order-parameter-based Monte Carlo simulation of crystallization," *J. Chem. Phys.* **124**, 134102 (2006).
- ⁶⁷R. Shekhar, J. K. Whitmer, R. Malshe, J. A. Moreno-Razo, T. F. Roberts, and J. J. de Pablo, "Isotropic–nematic phase transition in the Lebwohl–Lasher model from density of states simulations," *J. Chem. Phys.* **136**, 234503 (2012).
- ⁶⁸S. Singh, M. Chopra, and J. J. de Pablo, "Density of States–Based Molecular Simulations," *Annu. Rev. Chem. Biomol. Eng.* **3**, 369–394 (2012).
- ⁶⁹H. Sidky and J. K. Whitmer, "Elastic properties of common Gay–Berne nematogens from density of states (DOS) simulations," *Liq. Cryst.* **43**, 2285–2299 (2016).
- ⁷⁰H. Fu, H. Chen, X. Wang, H. Chai, X. Shao, W. Cai, and C. Chipot, "Finding an Optimal Pathway on a Multidimensional Free-Energy Landscape," *J. Chem. Inf. Model.* **60**, 5366–5374 (2020).
- ⁷¹N. C. Karayiannis, K. Foteinopoulou, and M. Laso, "Entropy-Driven Crystallization in Dense Systems of Athermal Chain Molecules," *Phys. Rev. Lett.* **103**, 045703 (2009).
- ⁷²S. Torquato, T. M. Truskett, and P. G. Debenedetti, "Is Random Close Packing of Spheres Well Defined?" *Phys. Rev. Lett.* **84**, 2064–2067 (2000).
- ⁷³J. J. de Pablo, M. Laso, J. I. Siepmann, and U. W. Suter, "Continuum-configurational-bias Monte Carlo simulations of long-chain alkanes," *Mol. Phys.* **80**, 55–63 (1993).
- ⁷⁴J. J. de Pablo, M. Laso, U. W. Suter, and H. D. Cochran, "Continuum configurational bias Monte-Carlo studies of alkanes and polyethylene," *Fluid Phase Equilib.* **83**, 323–331 (1993).
- ⁷⁵P. V. K. Pant and D. N. Theodorou, "Variable Connectivity Method for the Atomistic Monte Carlo Simulation of Polydisperse Polymer Melts," *Macromolecules* **28**, 7224–7234 (1995).
- ⁷⁶F. A. Escobedo and J. J. de Pablo, "Extended continuum configurational bias Monte Carlo methods for simulation of flexible molecules," *J. Chem. Phys.* **102**, 2636–2652 (1995).
- ⁷⁷V. G. Mavrantzas, T. D. Boone, E. Zervopoulou, and D. N. Theodorou, "End-Bridging Monte Carlo: A Fast Algorithm for Atomistic Simulation of Condensed Phases of Long Polymer Chains," *Macromolecules* **32**, 5072–5096 (1999).
- ⁷⁸A. Uhlherr, V. G. Mavrantzas, M. Doxastakis, and D. N. Theodorou, "Directed Bridging Methods for Fast Atomistic Monte Carlo Simulations of Bulk Polymers," *Macromolecules* **34**, 8554–8568 (2001).
- ⁷⁹O. Alexiadis, V. G. Mavrantzas, R. Khare, J. Beckers, and A. R. C. Baljon, "End-Bridging Monte Carlo Simulation of Bulk and Grafted Amorphous Polyethylene Above and Below the Glass Transition," *Macromolecules* **41**, 987–996 (2008).
- ⁸⁰K. A. Maerzke, L. Gai, P. T. Cummings, and C. McCabe, "Incorporating configurational-bias Monte Carlo into the Wang-Landau algorithm for continuous molecular systems," *J. Chem. Phys.* **137**, 204105 (2012).
- ⁸¹S. K. Kumar, M. Vacatello, and D. Y. Yoon, "Off-lattice Monte Carlo simulations of polymer melts confined between two plates," *J. Chem. Phys.* **89**, 5206–5215 (1988).
- ⁸²X. Li and Y. C. Chiew, "Monte Carlo simulation of Lennard-Jones chains," *J. Chem. Phys.* **101**, 2522–2531 (1994).
- ⁸³F. T. Wall and F. Mandel, "Macromolecular dimensions obtained by an efficient Monte Carlo method without sample attrition," *J. Chem. Phys.* **63**, 4592–4595 (1975).
- ⁸⁴E. B. Kim, R. Faller, Q. Yan, N. L. Abbott, and J. J. de Pablo, "Potential of mean force between a spherical particle suspended in a nematic liquid crystal and a substrate," *J. Chem. Phys.* **117**, 7781–7787 (2002).
- ⁸⁵L. Janosi and M. Doxastakis, "Accelerating flat-histogram methods for potential of mean force calculations," *J. Chem. Phys.* **131**, 054105 (2009).
- ⁸⁶E. A. Mastny and J. J. de Pablo, "Direct calculation of solid-liquid equilibria from density-of-states Monte Carlo simulations," *J. Chem. Phys.* **122**, 124109 (2005).

- ⁸⁷L. Maragliano, A. Fischer, E. Vanden-Eijnden, and G. Ciccotti, “String method in collective variables: Minimum free energy paths and isocommittor surfaces,” *J. Chem. Phys.* **125**, 024106 (2006).
- ⁸⁸D. Li and K. Zhang, “Unifying the concepts of scattering and structure factor in ordered and disordered samples,” *J. Appl. Crystallogr.* **54**, 644–660 (2021).
- ⁸⁹M. Engel, J. A. Anderson, S. C. Glotzer, M. Isobe, E. P. Bernard, and W. Krauth, “Hard-disk equation of state: First-order liquid-hexatic transition in two dimensions with three simulation methods,” *Phys. Rev. E* **87**, 042134 (2013).
- ⁹⁰K. Iland, J. Wölk, R. Strey, and D. Kashchiev, “Argon nucleation in a cryogenic nucleation pulse chamber,” *J. Chem. Phys.* **127**, 154506 (2007).
- ⁹¹D. Moroni, P. R. ten Wolde, and P. G. Bolhuis, “Interplay between Structure and Size in a Critical Crystal Nucleus,” *Phys. Rev. Lett.* **94**, 235703 (2005).
- ⁹²B. Peters and B. L. Trout, “Obtaining reaction coordinates by likelihood maximization,” *J. Chem. Phys.* **125**, 054108 (2006).
- ⁹³F. Trudu, D. Donadio, and M. Parrinello, “Freezing of a Lennard-Jones Fluid: From Nucleation to Spinodal Regime,” *Phys. Rev. Lett.* **97**, 105701 (2006).
- ⁹⁴T. Zykova-Timan, C. Valeriani, E. Sanz, D. Frenkel, and E. Tosatti, “Irreducible Finite-Size Effects in the Surface Free Energy of NaCl Crystals from Crystal-Nucleation Data,” *Phys. Rev. Lett.* **100**, 036103 (2008).
- ⁹⁵W. Lechner, C. Dellago, and P. G. Bolhuis, “Role of the Prestructured Surface Cloud in Crystal Nucleation,” *Phys. Rev. Lett.* **106**, 085701 (2011).
- ⁹⁶A. V. Brukhno, J. Anwar, R. Davidchack, and R. Handel, “Challenges in molecular simulation of homogeneous ice nucleation,” *J. Phys. Condens. Matter* **20**, 494243 (2008).
- ⁹⁷J. C. Palmer, F. Martelli, Y. Liu, R. Car, A. Z. Panagiotopoulos, and P. G. Debenedetti, “Metastable liquid–liquid transition in a molecular model of water,” *Nature* **510**, 385–388 (2014).
- ⁹⁸A. Haji-Akbari and P. G. Debenedetti, “Direct calculation of ice homogeneous nucleation rate for a molecular model of water,” *Proc. Natl. Acad. Sci.* **112**, 10582–10588 (2015).
- ⁹⁹S. Prestipino, A. Laio, and E. Tosatti, “Shape and area fluctuation effects on nucleation theory,” *J. Chem. Phys.* **140**, 094501 (2014).
- ¹⁰⁰J. F. Lutsko and M. A. Durán-Olivencia, “A two-parameter extension of classical nucleation theory,” *J. Phys. Condens. Matter* **27**, 235101 (2015).
- ¹⁰¹J. Russo and H. Tanaka, “Crystal nucleation as the ordering of multiple order parameters,” *J. Chem. Phys.* **145**, 211801 (2016).
- ¹⁰²J. Russo and H. Tanaka, “Nonclassical pathways of crystallization in colloidal systems,” *MRS Bulletin* **41**, 369–374 (2016).
- ¹⁰³N. C. Karayiannis, K. Foteinopoulou, C. F. Abrams, and M. Laso, “Modeling of crystal nucleation and growth in athermal polymers: self-assembly of layered nano-morphologies,” *Soft Matter* **6**, 2160–2173 (2010).
- ¹⁰⁴M. Anwar, F. Turci, and T. Schilling, “Crystallization mechanism in melts of short n-alkane chains,” *J. Chem. Phys.* **139**, 214904 (2013).
- ¹⁰⁵M. Anwar, J. T. Berryman, and T. Schilling, “Crystal nucleation mechanism in melts of short polymer chains under quiescent conditions and under shear flow,” *J. Chem. Phys.* **141**, 124910 (2014).
- ¹⁰⁶M. Anwar and T. Schilling, “Crystallization of polyethylene: A molecular dynamics simulation study of the nucleation and growth mechanisms,” *Polymer* **76**, 307–312 (2015).
- ¹⁰⁷X. Tang, F. Tian, T. Xu, L. Li, and A. Reinhardt, “Numerical calculation of free-energy barriers for entangled polymer nucleation,” *J. Chem. Phys.* **152**, 224904 (2020).

Semiflexible Oligomers Crystallize via a Cooperative Phase Transition – Supplementary Material

Pierre Kawak, Dakota S. Banks, Douglas R. Tree

Department of Chemical Engineering, Brigham Young University, Provo, Utah

Dated: November 1, 2021

1 Extended Methods

1.1 Markov-Chain Monte Carlo Simulations

We calculate melting curves using NVT-ensemble MCMC simulations. In MCMC simulations, a configuration of coarse-grained bead positions evolves as a series of “moves” are proposed and either accepted or rejected.¹ MCMC accepts moves using the Metropolis criterion to follow the Boltzmann distribution

$$P_{\text{acc}} = \min [1, \exp(-\Delta U/T_r)] \quad (1)$$

where $\Delta U = U_{\text{new}} - U_{\text{old}}$ is the change in total potential energy resulting from the proposed move.

We employ a variety of polymer-specific moves²⁻⁹ to ensure efficient equilibration of the polymer chains including: kink,^{10,11} end-kink,¹¹ reptation,^{10,12} and configurational-bias versions of the same.^{2,3,5,9} MCMC simulations use 50% kink, 25% configurational bias end-kink, and 25% configurational-bias reptation moves, unless otherwise noted. Configurational bias move versions use 25 trial moves. A similar set of moves are used for all of the other MC algorithms (e.g. WLMC, EXEDOS) described in this section.

Melting curves consist of order parameters $P_2(T_r)$ and $Q_6(T_r)$ at fixed ϕ , and melting was determined to take place at the step-change in value. Melting curves are calculated using MCMC according to the following procedure. MCMC simulations are initialized with a perfect crystalline (close packed and nematically aligned) initial configuration. The simulation proceeds at a fixed temperature and simulation box size until the system equilibrates. We determine equilibration in an MCMC simulations using an energy autocorrelation function. Simulations are considered well-equilibrated after they surpass ten times the autocorrelation time before stopping. Melting curves were obtained by sweeping temperature over the range $T \in [0.1, 1.0]$ at a fixed volume fraction, with melting curves calculated for volume fractions $\phi \in [0.379, 0.471]$. Eight independent replicates were performed at each value of T_r and ϕ to obtain error estimates. These error estimates are depicted on melting curves as error bars using standard error of the mean. Note that configurations from MCMC simulations were used as a source for initial configurations for WLMC and EXEDOS runs.

1.2 Wang Landau Simulations

WLMC simulations are a special type of MC method that directly calculate the system’s density of states, Ω ¹³⁻¹⁸. As a “flat-histogram” method, WLMC simulations are excellent at sampling rare events such as crystallization. In principle, a single (but very long) WLMC simulation can calculate the entire density of states. As such, WLMC simulations run at fixed ϕ , but give results that span temperature. Consequently, Ω can be used to construct the heat capacity, which can be used to determine phase transitions. Through canonical analysis, one can also determine the temperature-dependent behavior of other order parameters (i.e. melting curves).

Similar to MCMC, WLMC proceeds via a trial move and a choice of acceptance or rejection. We use the same moveset in WLMC as discussed above. However, the WLMC acceptance probability promotes equal visits to all states of a system and is of the form

$$P_{\text{acc}} = \min \left[1, \frac{\Omega(U_{\text{old}})}{\Omega(U_{\text{new}})} \right] \quad (2)$$

where $\Omega(U_i)$ is the value of the density of states for a configuration with potential energy U_i . The density of states used in the acceptance criteria is also the principal product of the WLMC simulation. $\Omega(U_i)$ is initially assumed to be unity for all U_i and when the simulation visits U_{new} , $\Omega(U_{\text{new}})$ is increased by multiplying it with a modification factor, f . The WLMC algorithm proceeds until it has uniformly visited all accessible states of the system. We determine the latter using a histogram of U_i , and terminate the simulation when all states have been visited, and the deviation of the minimum and average number of visits is less than 20%.

Execution of the above procedure generates only a rough estimate of Ω , whose accuracy is limited by the value of f . Subsequent iterations of the above process are necessary to obtain an accurate value of Ω . By convention, $f_1 = e$ and $f_n = \sqrt{f_{n-1}}$ where the subscript n denotes the WLMC iteration number.¹³ We use 27 WLMC iterations in our calculations, giving a modification factor (and error estimate) of $f = 1 + 10^{-8}$ on the final iteration.

While a single long WLMC simulation can in principle determine Ω , such a method is too costly for a system larger than a few beads. To speed convergence, the simulation space is divided into overlapping windows and each window is given multiple “walkers”, i.e. replicate

WLMC simulations that run in parallel in the same window. In WLMC, Ω is only determined to within an additive constant, so linear regression is used to “stitch” overlapping windows together to obtain a master curve. In our calculations, we divide the internal energy space $U/\epsilon \in [-720, 0]$ into 15-18 windows with 8-16 walkers in each window, for a total of 120-288 total processors committed to the simulation depending on the difficulty of the simulation. Note that each of the walkers must be seeded with an independent initial configuration that obeys the energy constraints of the window. These initial configurations were generated using MCMC simulations as described above.

Landau and coworkers proposed yet further improvements to the WLMC method using replica-exchange principles.¹⁹⁻²² Consider two walkers, α and β , with respective configurations A and B that reside in neighboring windows. If the energies of these configurations $U_A = U(A)$ and $U_B = U(B)$ are within the overlap region between the two windows, they may swap configurations according the acceptance criteria²²

$$P_{\text{acc}} = \min \left[1, \frac{\Omega_\alpha(U_A)\Omega_\beta(U_B)}{\Omega_\alpha(U_B)\Omega_\beta(U_A)} \right] \quad (3)$$

In such simulations, each walker maintains a separate, local estimate of Ω and a separate histogram. These are averaged, and when the global histogram is flat, the global Ω is re-distributed among all walkers and a new WLMC iteration starts.

We implemented multiple walker replica-exchange Wang Landau (REWL) simulations, and in our experience they speed convergence via parallelization and through improved sampling efficiency. A well-known problem in the WLMC algorithm is that single walkers get “stuck” due to hidden barriers and can oversample certain regions of phase space. Multiple independent walkers partially solve this problem, because each independent replica begins in a different initial state and is unlikely to be trapped by the same hidden barriers. The configuration exchange in REWL simulations samples a wider range of phase space creating walkers that are even more efficient at overcoming these hidden barriers. Exchange between windows also improves the ergodicity of the simulation, allowing walkers to explore an energy range that is larger than a single window.

As mentioned, classical formulas from statistical mechanics can be used to convert the information embedded in Ω to other metrics. We use the formula for the fixed-volume heat

capacity,

$$C_V(T) = \frac{\langle U^2 \rangle - \langle U \rangle^2}{kT^2} \quad (4)$$

The moments of U are calculated via

$$\langle U^n \rangle(T) = \frac{\sum_i U_i^n \exp(\ln \Omega_i - U_i/kT)}{\sum_i \exp(\ln \Omega_i - U_i/kT)} \quad (5)$$

where i indexes discrete states of $U \in [U_{\min}, 0]$ and $\Omega_i = \Omega(U_i)$. We also calculate melting curves using WLMC via the formula

$$\langle M \rangle(T) = \frac{\sum_i \langle M_i \rangle \exp(\ln \Omega_i - U_i/kT)}{\sum_i \exp(\ln \Omega_i - U_i/kT)} \quad (6)$$

where $M(T)$ is an order parameter such as P_2 or Q_6 and $M_i = M(U_i)$.²³ Discontinuities in U , Q_6 and P_2 melting curves happen at the first order melting/crystallization transition and can be used to identify T_m .

1.3 Expanded Ensemble Density of States Simulations

EXEDOS is a modified WLMC approach that builds the FEL along a certain order parameter or reaction coordinate.²⁴ Unlike WLMC where Ω is a function of internal energy, the density of states in EXEDOS is a function of an order parameter. EXEDOS has been previously used to construct an FEL along a variety of order parameters including distance,^{24–26} cutoff radii,¹⁷ Steinhardt order parameters,²⁷ and nematic alignment.^{28,29} EXEDOS simulations mirror the WLMC method, except the acceptance rate is given by

$$P_{\text{acc}} = \min \left[1, \frac{Z(\theta_{\text{old}})}{Z(\theta_{\text{new}})} \exp(-\Delta U/kT) \right] \quad (7)$$

where Z is the “expanded ensemble” density of states, θ is a generic order parameter and $\Delta U = U_{\text{new}} - U_{\text{old}}$. Note that unlike WLMC simulations, EXEDOS simulations are in the NVT ensemble and therefore have a defined temperature. The free energy as a function of the order parameter θ (the FEL) is given by

$$F(\theta) = -kT \ln Z(\theta) + C \quad (8)$$

where C is an arbitrary constant.

In our calculations, we computed two-dimensional (2D) FELs from $Z(P_2, Q_6)$, using EXEDOS simulations that span two order parameters. These calculations employed an identical moveset to those described in Section 1.1 and a similar multiple window/multiple walker scheme to the one described in Section 1.2. We also used replica-exchange techniques in our EXEDOS simulations. The acceptance probability in such simulations are even simpler than WLMC with $P_{\text{acc}} = 1$ for walkers in overlapping windows.²⁶

In addition to our simulations spanning several autocorrelation times, all other metrics demonstrate that our results are valid and reproducible. For instance, small variations in chosen bin sizes and overall ranges of order parameters do not affect our free energy results significantly. Additionally, differently set up simulations such as differently windowed or replicated ones yield similar FELs. Select WLMC experiments featuring spontaneous crystallization from a disordered melt yield similar melting curves as simulations seeded from crystals like the protocols used in this study ($O(0.001)$). This grants us confidence in our estimates of T_m used in EXEDOS simulations. These factors and the well-replicated replica-exchange techniques we use assure us of the validity of our results despite difficulties in simulating this dense hard sphere system.

Our interest in the FEL extends to an analysis of its topological features with basins representing stable or metastable states and peaks representing rare events. Based on ideas from classical nucleation theory and transition state theory, we expect the minimum free energy path (MFEP) between basins to be indicative of the kinetics of the system.³⁰ Similarly, we expect the maximum of the MFEP (a saddle point on the FEL surface) to characterize the primary barrier to nucleation. To find the MFEP and the saddle point, we used the “multidimensional lowest energy” (MULE) algorithm recently developed by Fu et al.³¹ We use the resulting MFEP to calculate the barrier height between the saddle point and basins.

1.4 Order Parameters and Structure Factor

We characterize the phase behavior of the simulated system using the order parameters Q_6 and P_2 . Q_6 is a Steinhardt order parameter that measures the local positional order of a bead with its neighbors based on spherical harmonics and we use it to characterize

crystallinity. P_2 is the second Legendre polynomial and measures nematic alignment with the surrounding environment. We also investigated other order parameters not discussed here (e.g. the Steinhard parameter Q_4), but our calculations show that Q_6 and P_2 are sufficient to capture the phase behavior of this system.

To compute Q_6 ,³² one first calculates a local order parameter q_6 for bead i ,

$$q_{6m}(i) = \frac{1}{N_{\text{fb}}(i)} \sum_{j=1}^{N_{\text{fb}}(i)} Y_{6m}(\mathbf{r}_{ij}) \quad (9)$$

$$q_6(i) = \left[\frac{4\pi}{13} \sum_{m=-6}^6 |q_{6m}(i)|^2 \right]^{1/2} \quad (10)$$

where $N_{\text{fb}}(i)$ is the number of nearest neighbors of bead i (in our implementation, $N_{\text{fb}}(i) = 6$ for all cases here). Y_{6m} is the spherical harmonic function of degree six and order m with respect to the j^{th} neighboring bead with displacement vector $\mathbf{r}_{ij} = \mathbf{r}_j - \mathbf{r}_i$. If a bead does not have six neighbors within a radial distance of 1.3σ , it is considered non-crystalline, and its q_6 is set to zero. The global parameter Q_6 is the average of the value of q_6 for all beads,

$$Q_6 = \frac{1}{N_{\text{tot}}} \sum_{i=1}^{N_{\text{tot}}} q_6(i) \quad (11)$$

where $N_{\text{tot}} = N_b N_c$ is the total number of beads in the system. The values of Q_6 that indicate crystalline or melt behavior depends on density but a larger value generally indicates higher crystalline order.

The nematic order parameter P_2 is more easily calculated. Again, we define a local order parameter,

$$p_2(i) = \frac{3}{2} \langle \cos^2 \theta_{ij} \rangle_i - \frac{1}{2} \quad (12)$$

where θ_{ij} is the angle made between bond vectors \mathbf{b}_i and \mathbf{b}_j , and the average $\langle \rangle_i$ is over all j neighbors within a distance of 1.3σ from bead i . The bond vector of bead i is defined as $\mathbf{b}_i = \mathbf{r}_i - \mathbf{r}_{i-1}$. The global value of P_2 is also calculated as an average over all beads,

$$P_2 = \frac{1}{N_{\text{tot}}} \sum_{i=1}^{N_{\text{tot}}} p_2(i) \quad (13)$$

A value of P_2 closer to one indicates nematic alignment, whereas a value close to zero signifies a random distribution of chains.

Note that both of these order parameters are “global”, in that they characterize the crystalline and nematic order of the entire system. It has been shown for large systems that local order parameters are more appropriate for characterizing nucleation behavior and comparing to classical nucleation theory.³³ However, the system in question here is too small for the difference to be meaningful. The critical nucleus is large relative to the simulation box, and crystallization proceeds in the entire box simultaneously.

The structure factor is a useful measure of orientational and positional order of a material, and gives information equivalent to SAXS and WAXS experiments. We compute the structure factor of a single configuration using

$$S(\mathbf{q}) = \frac{1}{N_c N_b} \sum_{j=1}^{N_c N_b} |\exp(i\mathbf{q} \cdot \mathbf{r}_j)|^2 \quad (14)$$

In the main text, 2D structure factors are given by averaging over the third dimension. In addition, these structure factors are *ensemble-averaged* structure factors and are averaged over many configurations.

1.5 Windowing Scheme in 2D EXEDOS Simulations

In EXEDOS windowing, we divide the entire P_2 range into overlapping windows that all span the entire range of Q_6 . This choice was made through a trial-and-error process of what achieves the most efficient convergence. We found that the free energy change ($-kT \ln(\Omega)$) along P_2 is far larger at constant Q_6 than vice versa. This is due to the large energy change when aligning chains versus when fitting them into a crystalline lattice. Accordingly, P_2 bins are smaller in size relative to the total range and are used to window the simulation.

The windowing procedure for the P_2 range was also based on a trial-and-error process and depended on difficulty. In other words, higher ϕ simulations required more windows. Accordingly, the P_2 range ($\approx \in [0.0, 0.928]$) was divided up into 21–29 equally-sized windows. The P_2 bin size was set equal to 0.00032 making the overall P_2 range fit into 2900 bins. For each ϕ , this discretization is shown in Table S1.

As mentioned, every window spanned the entire relevant range of Q_6 at any single ϕ . As can be seen from Table S1, the Q_6 range changes for each ϕ which is a deliberate choice

made based on the melting curves in the main text. The bin size was chosen to provide 5 Q_6 bins in total at each ϕ .

Table S1: Range of P_2 and Q_6 spanned in EXEDOS simulations at the studied ϕ .

ϕ	T	Q_6			P_2			Num. of Windows	Num. of Replicates
		Low	High	Bin	Low	High	Bin		
0.379	0.226	0.332	0.342	0.002	0.128	0.74432		19	2
0.407	0.248	0.396	0.411	0.003	0.16	0.8		20	
0.428	0.267	0.43	0.46	0.006	0.19776	0.968	0.00032	26	3
0.438	0.291		0.48	0.01	0.0	0.99424		32	
0.471	0.374	0.46	0.52	0.012		0.99008		33	

2 Markov Chain and Wang Landau Monte Carlo results

Like Figure 4 for $\phi = 0.438$, Figures S1, S2, S3 and S4 show the MCMC and WLMC U/ϵ , P_2 and Q_6 melting curves for $\phi = [0.471, 0.428, 0.407, 0.379]$, respectively. As discussed, each figure shows a single first order phase transition at the respective T_m (shown in the legend). Clearly, there is a difference between the melt-crystal transition in Figures 4, S1, S2 and the melt-nematic transition in Figures S3 and S4. The initial has a large P_2 change resulting in near unity values at low T_r and is well-described by changes in Q_6 . In contrast, the latter approaches lower P_2 values at low T_r and has small changes in Q_6 at the transition.

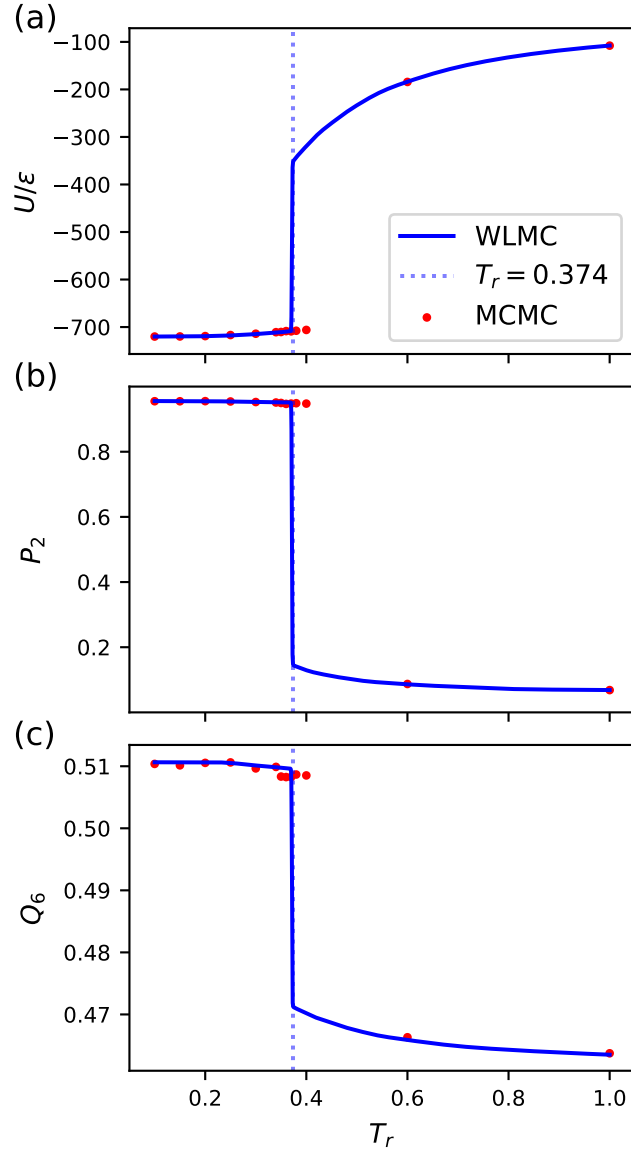


Figure S1: Melting curves of the (a) internal energy, (b) nematic order parameter, (c) crystalline order parameter versus reduced temperature from MCMC (red points) and WLMC (blue line) at $\phi = 0.471$. The vertical dashed line is the best estimate of the melting temperature ($T_m = 0.374$).

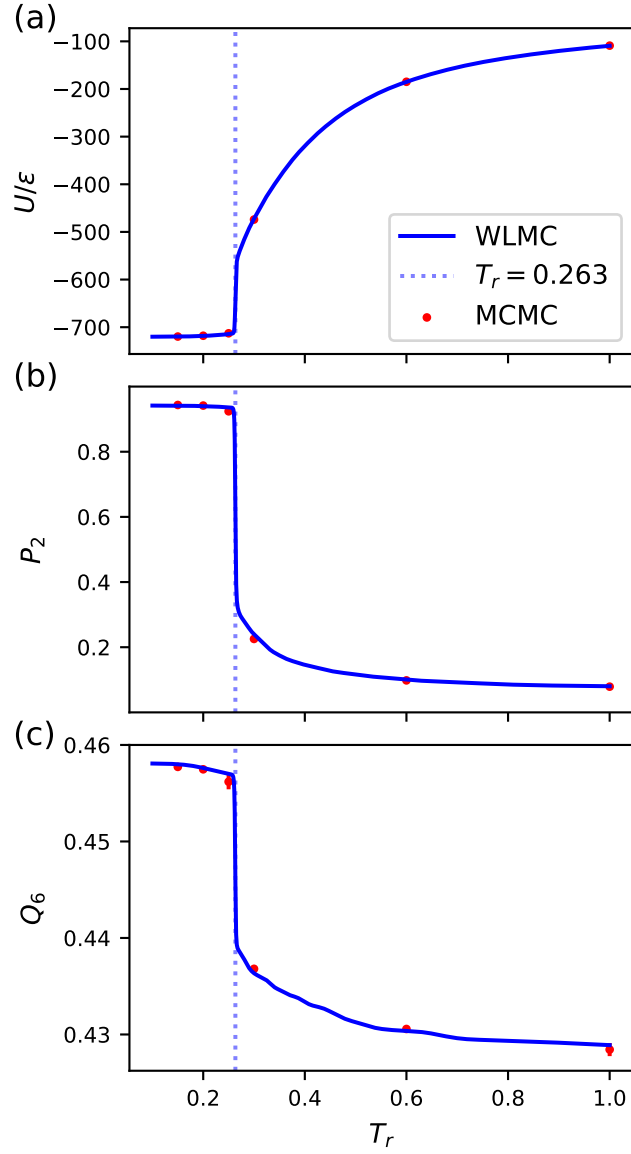


Figure S2: Melting curves of the (a) internal energy, (b) nematic order parameter, (c) crystalline order parameter versus reduced temperature from MCMC (red points) and WLMC (blue line) at $\phi = 0.428$. The vertical dashed line is the best estimate of the melting temperature ($T_m = 0.263$).

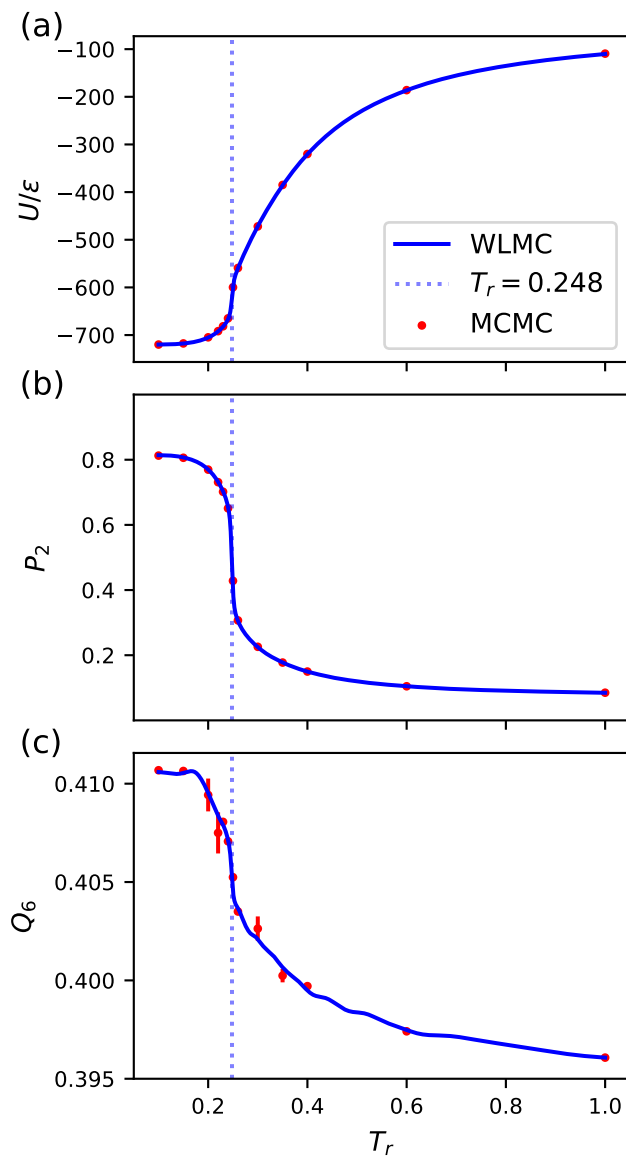


Figure S3: Melting curves of the (a) internal energy, (b) nematic order parameter, (c) crystalline order parameter versus reduced temperature from MCMC (red points) and WLMC (blue line) at $\phi = 0.407$. The vertical dashed line is the best estimate of the melting temperature ($T_m = 0.248$).

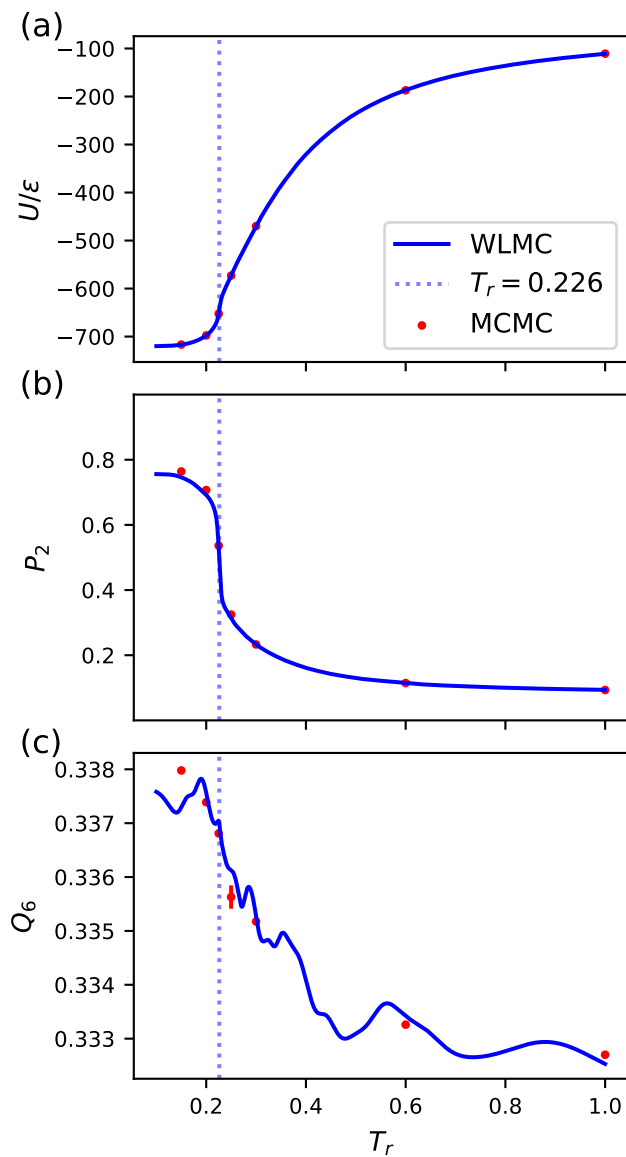


Figure S4: Melting curves of the (a) internal energy, (b) nematic order parameter, (c) crystalline order parameter versus reduced temperature from MCMC (red points) and WLMC (blue line) at $\phi = 0.379$. The vertical dashed line is the best estimate of the melting temperature ($T_m = 0.226$).

3 Minimum Free Energy Paths

As in Figure 9a for $\phi = 0.438$, Figures S5a, S6a, S7a and S8a show the MULE-extracted MFEP in yellow over FELs for $\phi = [0.471, 0.428, 0.407, 0.379]$, respectively. As discussed in the main text, crystallization transitions for $\phi = [0.471, 0.438, 0.428]$ require smooth and cooperative changes in P_2 and Q_6 whereas the latter transitions only require P_2 changes to transition at near-constant Q_6 . MFEP values projected along the arc-length in Q_6 - P_2 space are shown in Figures S5b, S6b, S7b and S8b for $\phi = [0.471, 0.428, 0.407, 0.379]$, respectively. These figures allow for the extraction of barrier heights $\Delta F^\ddagger/\epsilon$ from 2D EXEDOS simulations (compiled in Figure 10).

To help the reader visualize FEL differences between differing values of ϕ , and more importantly, between crystallization and nematic transitions, Figure 8 is reproduced here in two different presentation styles in Figures S9 and S10. Figure S9 shows the same P_2 domain for all figures while retaining the color bars used for each figure in the main text. Since data was not collected for the entire P_2 range in all ϕ FELs, regions with no collected data are displayed in white. This figure reveals the relative P_2 values of the basins in the FEL at different volume fractions. As ϕ increases, the low temperature basin (upper), decreases in P_2 , relative to the melt basin. This effect is exacerbated for the nematic transition, as discussed in the main text. Figure S10 keeps the same P_2 domain in all FELs as in Figure S9 but also no longer restrains the color bar to the main text and retains the same color bar among all ϕ FELs. The inclusion of the $\phi = 0.471$ FEL's data points at high P_2 (originally cut off for better visualization) increase its color bar maximum by 4. This has the effect of obscuring the shading in all FELs. As discussed in the main text and this figure shows, the free energy changes encountered in the FEL decrease as ϕ decreases. This manifests in the lower four ϕ FELs by a complete disappearance of the profile as the changes encountered in these figures $O(10) - O(10^{-2})$ are minuscule relative to the $\phi = 0.471$ FEL ($O(10^2)$).

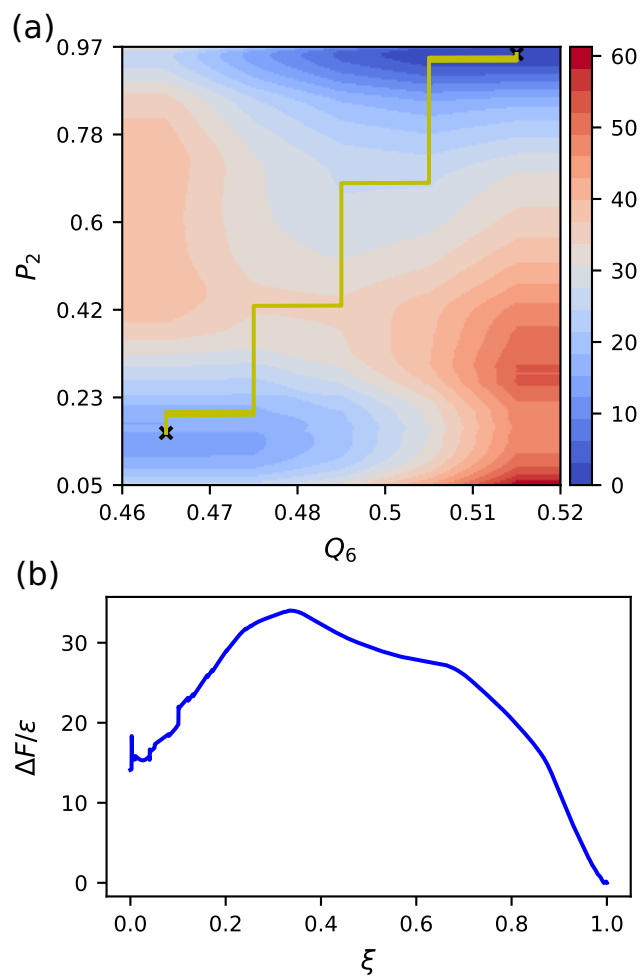


Figure S5: (a) 2D Q_6 - P_2 FEL at $\phi = 0.471$ with MULE-extracted MFEP in yellow. Discrete jumps in the MFEP are related to the discrete size of the bins along Q_6 . (b) MFEP values from the 2D Q_6 - P_2 FEL at $\phi = 0.471$ projected along the reaction coordinate of its arc-length in Q_6 - P_2 space.

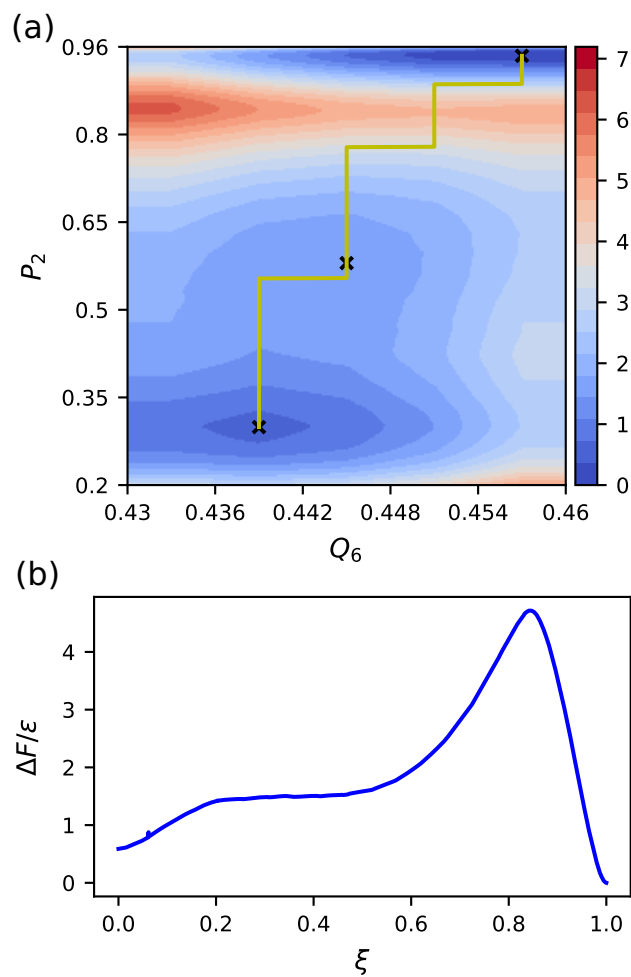


Figure S6: (a) 2D Q_6 - P_2 FEL at $\phi = 0.428$ with MULE-extracted MFEP in yellow. Discrete jumps in the MFEP are related to the discrete size of the bins along Q_6 . (b) MFEP values from the 2D Q_6 - P_2 FEL at $\phi = 0.428$ projected along the reaction coordinate of its arc-length in Q_6 - P_2 space.

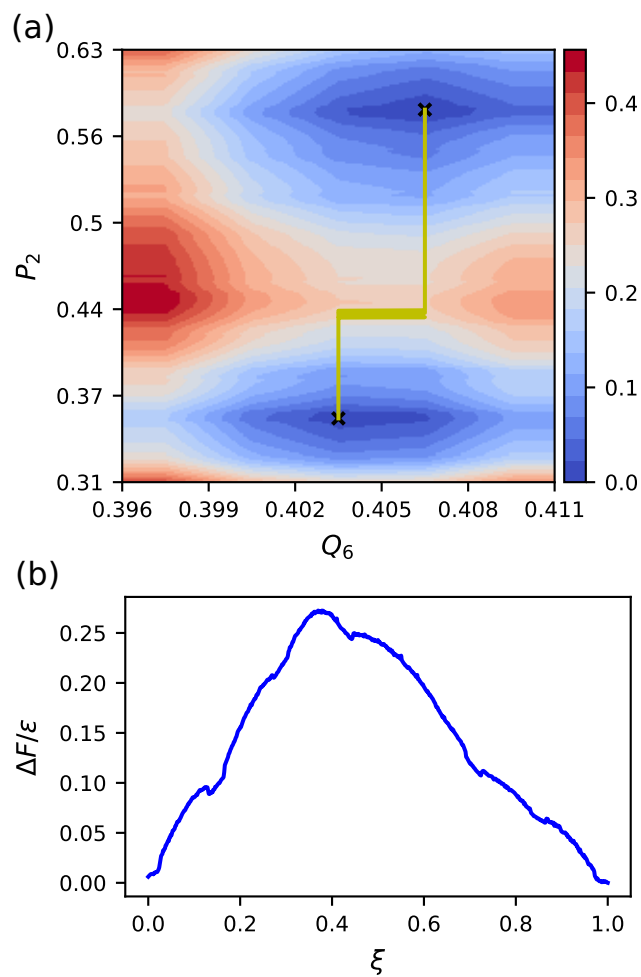


Figure S7: (a) 2D Q_6 - P_2 FEL at $\phi = 0.407$ with MULE-extracted MFEP in yellow. Discrete jumps in the MFEP are related to the discrete size of the bins along Q_6 . (b) MFEP values from the 2D Q_6 - P_2 FEL at $\phi = 0.407$ projected along the reaction coordinate of its arc-length in Q_6 - P_2 space.

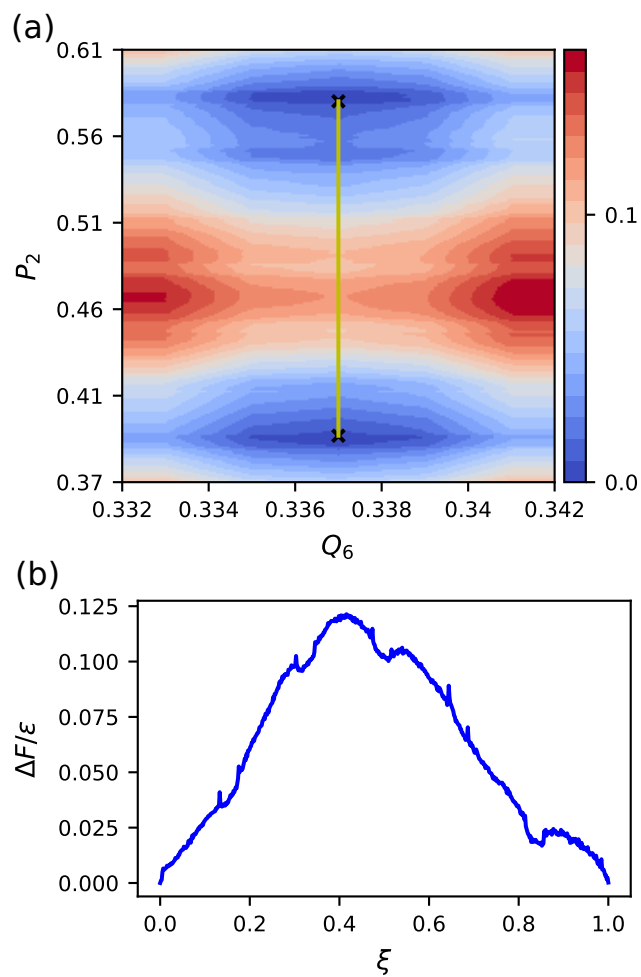


Figure S8: (a) 2D Q_6 - P_2 FEL at $\phi = 0.379$ with MULE-extracted MFEP in yellow. Discrete jumps in the MFEP are related to the discrete size of the bins along Q_6 . (b) MFEP values from the 2D Q_6 - P_2 FEL at $\phi = 0.379$ projected along the reaction coordinate of its arc-length in Q_6 - P_2 space.

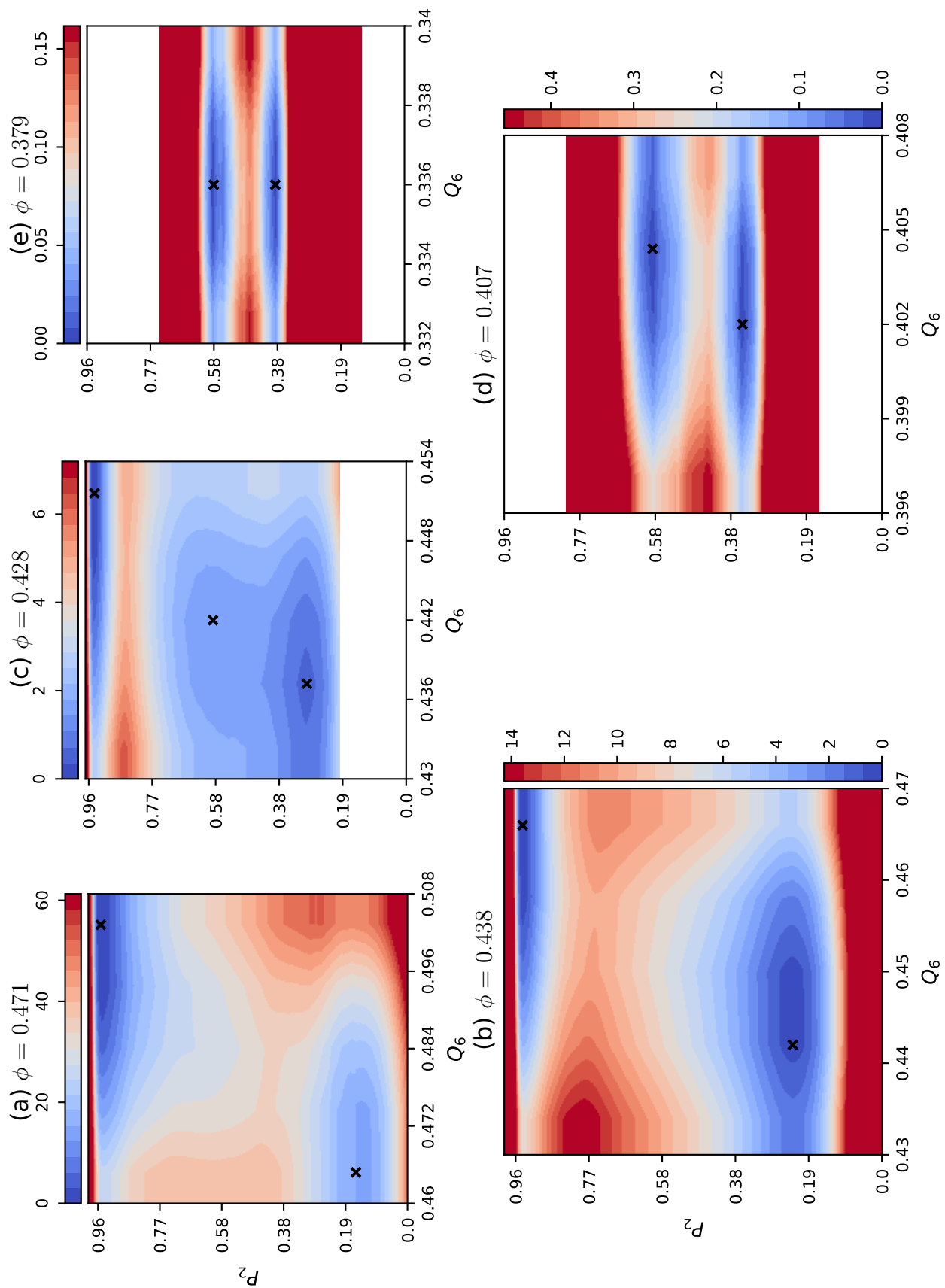


Figure S9: Same as FEL Figure in main text but with same P_2 domain for all FELs. Regions without collected data are white and red colors free energies above color bar maximum.

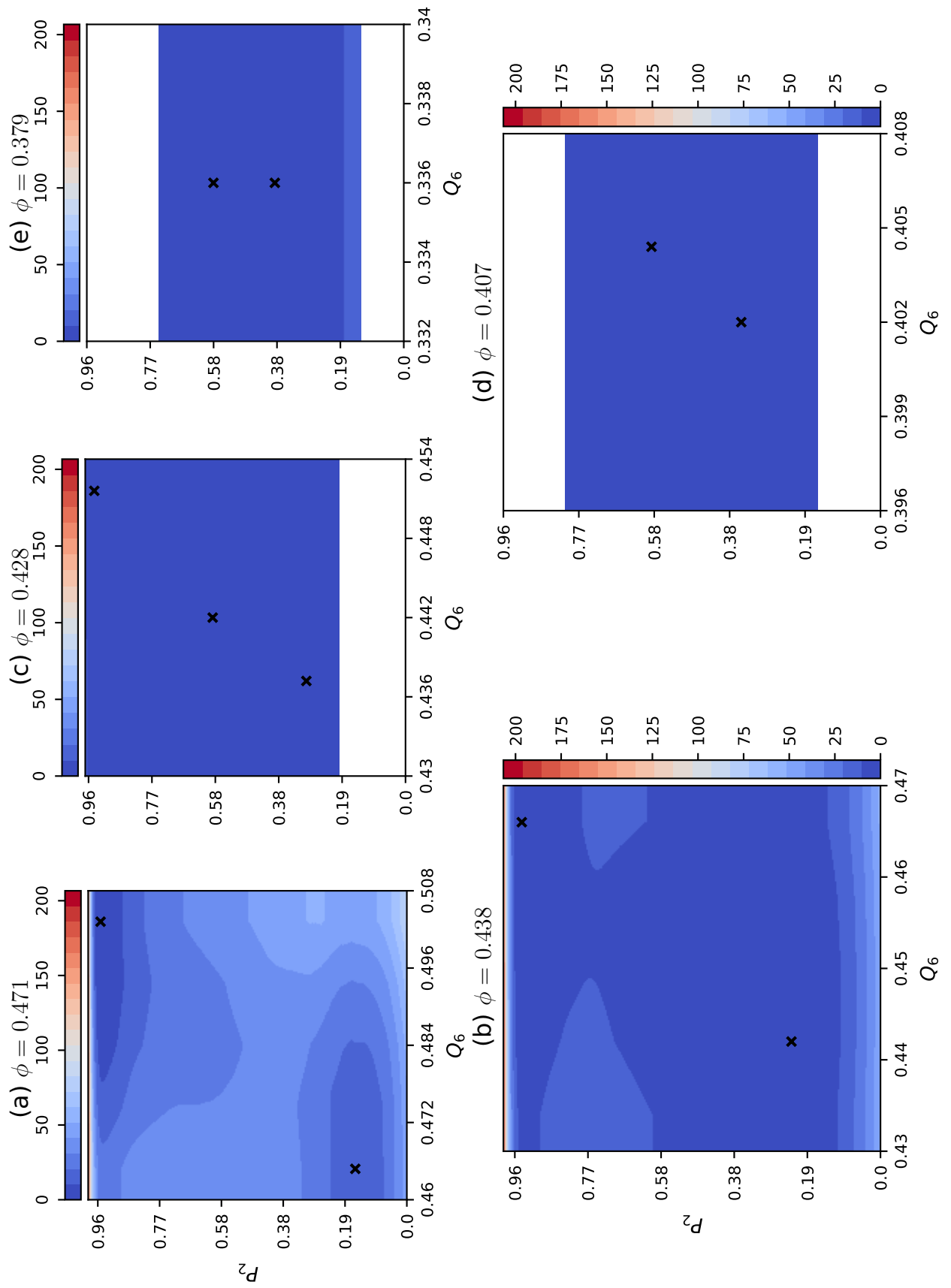


Figure S10: FEL figure with the same color bar range (0–80) and P_2 domain for all FELs.

References

1. D. Frenkel and B. Smit, *Understanding molecular simulation: From algorithms to applications* (Academic Press, 2002).
2. J. J. de Pablo, M. Laso, J. I. Siepmann, and U. W. Suter, *Mol. Phys.* **80**, 55 (1993).
3. J. J. de Pablo, M. Laso, U. W. Suter, and H. D. Cochran, *Fluid Phase Equilib.* **83**, 323 (1993).
4. P. V. K. Pant and D. N. Theodorou, *Macromolecules* **28**, 7224 (1995).
5. F. A. Escobedo and J. J. de Pablo, *J. Chem. Phys.* **102**, 2636 (1995).
6. V. G. Mavrantzas, T. D. Boone, E. Zervopoulou, and D. N. Theodorou, *Macromolecules* **32**, 5072-5096 (1999).
7. A. Uhlherr, V. G. Mavrantzas, M. Doxastakis, and D. N. Theodorou, *Macromolecules* **34**, 8554 (2001).
8. O. Alexiadis, V. G. Mavrantzas, R. Khare, J. Beckers, and A. R. C. Baljon, *Macromolecules* **41**, 987 (2008).
9. K. A. Maerzke, L. Gai, P. T. Cummings, and C. McCabe, *J. Chem. Phys.* **137**, 204105 (2012).
10. S. K. Kumar, M. Vacatello, and D. Y. Yoon, *J. Chem. Phys.* **89**, 5206 (1988).
11. X. Li and Y. C. Chiew, *J. Chem. Phys.* **101**, 2522 (1994).
12. F. T. Wall and F. Mandel, *J. Chem. Phys.* **63**, 4592 (1975).
13. F. Wang and D. P. Landau, *Phys. Rev. Lett.* **86**, 2050 (2001).
14. Q. Yan, R. Faller, and J. J. de Pablo, *J. Chem. Phys.* **116**, 8745 (2002).
15. R. Faller and J. J. de Pablo, *J. Chem. Phys.* **119**, 4405 (2003).
16. N. Rathore, T. A. Knotts, and J. J. de Pablo, *J. Chem. Phys.* **118**, 4285 (2003).
17. E. A. Mastny and J. J. de Pablo, *J. Chem. Phys.* **122**, 124109 (2005).
18. B. J. Schulz, K. Binder, and M. Müller, *Phys. Rev. E* **71**, 46705 (2005).
19. T. Vogel, Y. W. Li, T. Wüst, and D. P. Landau, *Phys. Rev. Lett.* **110**, 210603 (2013).
20. T. Vogel, Y. W. Li, T. Wüst, and D. P. Landau, *Phys. Rev. E* **90**, 023302 (2014).
21. G. Shi, T. Vogel, T. Wüst, Y. W. Li, and D. P. Landau, *Phys. Rev. E* **90**, 033307 (2014).

22. Y. W. Li, T. Vogel, T. Wüst, and D. P. Landau, *J. Phys. Conf. Ser.* **510**, 012012 (2014).
23. D. A. McQuarrie, *Statistical Mechanics* (University Science Books, 2000).
24. E. B. Kim, R. Faller, Q. Yan, N. L. Abbott, and J. J. de Pablo, *J. Chem. Phys.* **117**, 7781 (2002).
25. N. Rathore, Q. Yan, and J. J. de Pablo, *J. Chem. Phys.* **120**, 5781 (2004).
26. L. Janosi and M. Doxastakis, *J. Chem. Phys.* **131**, 054105 (2009).
27. M. Chopra, M. Müller, and J. J. de Pablo, *J. Chem. Phys.* **124**, 134102 (2006).
28. R. Shekhar, J. K. Whitmer, R. Malshe, J. A. Moreno-Razo, T. F. Roberts, and J. J. de Pablo, *J. Chem. Phys.* **136**, 234503 (2012).
29. H. Sidky and J. K. Whitmer, *Liq. Cryst.* **43**, 2285 (2016).
30. L. Maragliano, A. Fischer, E. Vanden-Eijnden, and G. Ciccotti, *J. Chem. Phys.* **125**, 024106 (2006).
31. H. Fu, H. Chen, X. Wang, H. Chai, X. Shao, W. Cai, and C. Chipot, *J. Chem. Inf. Model.* **60**, 5366 (2020).
32. P. J. Steinhardt, D. R. Nelson, and M. Ronchetti, *Phys. Rev. B* **28**, 784 (1983).
33. A. Reinhardt, J. P. K. K. Doye, E. G. Noya, and C. Vega, *J. Chem. Phys.* **137**, 194504 (2012).